

Combined Optical and Radio-Frequency Perspectives on Hybrid Cloud-to-Ground Lightning Observed by the FORTE Satellite

Michael Jay Peterson¹, Tracy Ellen Lavezzi Light², and Xuan-Min Shao²

¹ISR-2, Los Alamos National Laboratory

²Los Alamos National Laboratory (DOE)

November 22, 2022

Abstract

We use the coincident optical and radio-frequency measurements taken by the FORTE satellite to shed light on common optical signatures recorded by NASA and NOAA lightning imagers during Cloud-to-Ground (CG) lightning. We build flash cluster data for FORTE using the same clustering techniques as GLM and document the optical / RF evolution of an oceanic hybrid -CG flash over its 656 ms duration. The flash began with strong VHF emission from a Narrow Bipolar Event (NBE) that initiated a period of normal bilevel intracloud (IC) activity in two vertical layers (8 km and 12 km) that lasted for 490 ms. VHF waveforms show step leader activity ahead of seawater attachment in the return stroke. All impulsive VHF sources after the stroke come from the lower (8 km layer) only. K-changes are noted following the return stroke, but no subsequent strokes are detected. The optical flash began 136 ms after the NBE RF pulse. 22 of the 30 optical groups were dim and occurred during the in-cloud phase of the flash. This activity included both isolated pulses and sustained periods of illumination over tens of milliseconds. Initial cloud pulses accounted for 23% of the total optical radiance from the flash. Illumination during the return stroke contributed a further 58% of the total radiance, and the K-changes and cloud pulses after the stroke supplied the remaining 19%. These results highlight the benefit of having RF alongside optical lightning measurements for clarifying signatures in the optical data and providing information on their physical origins.

1 **Combined Optical and Radio-Frequency Perspectives on Hybrid Cloud-to-Ground**
2 **Lightning Observed by the FORTE Satellite**

3
4 **Michael Peterson¹, Tracy E. L. Light¹, Xuan-Min Shao¹**

5
6
7 ¹ISR-2, Los Alamos National Laboratory, Los Alamos, New Mexico

8
9
10
11
12
13 Corresponding author: Michael Peterson (mpeterson@lanl.gov), B241, P.O. Box 1663 Los
14 Alamos, NM, 87545

15
16
17 **Key Points:**

- 18 • The FORTE satellite included optical and RF payloads for measuring transient signals,
19 including a CCD imager based on the design used with OTD/LIS/GLM
- 20 • Flash cluster data is produced for FORTE that includes fast photodiode and RF events
21 incorporated into the cluster feature data tree
- 22 • Optical / RF measurements are used to examine cloud pulses, the return stroke, and
23 subsequent K-changes in an oceanic hybrid CG flash

24 **Abstract**

25

26 We use the coincident optical and radio-frequency measurements taken by the FORTE
27 satellite to shed light on common optical signatures recorded by NASA and NOAA lightning
28 imagers during Cloud-to-Ground (CG) lightning. We build flash cluster data for FORTE using
29 the same clustering techniques as GLM and document the optical / RF evolution of an oceanic
30 hybrid -CG flash over its 656 ms duration. The flash began with strong VHF emission from a
31 Narrow Bipolar Event (NBE) that initiated a period of normal bilevel intracloud (IC) activity in
32 two vertical layers (8 km and 12 km) that lasted for 490 ms. VHF waveforms show step leader
33 activity ahead of seawater attachment in the return stroke. All impulsive VHF sources after the
34 stroke come from the lower (8 km layer) only. K-changes are noted following the return stroke,
35 but no subsequent strokes are detected.

36 The optical flash began 136 ms after the NBE RF pulse. 22 of the 30 optical groups were
37 dim and occurred during the in-cloud phase of the flash. This activity included both isolated
38 pulses and sustained periods of illumination over tens of milliseconds. Initial cloud pulses
39 accounted for 23% of the total optical radiance from the flash. Illumination during the return
40 stroke contributed a further 58% of the total radiance, and the K-changes and cloud pulses after
41 the stroke supplied the remaining 19%. These results highlight the benefit of having RF
42 alongside optical lightning measurements for clarifying signatures in the optical data and
43 providing information on their physical origins.

44

45

46 **Plain Language Summary**

47

48 Lightning has been measured from space for more than 25 years. Most space-based
49 sensors were optical instruments that detect lightning by looking for the cloud-top lighting up.
50 Recent studies have shown that we can measure how lightning moves using this type of
51 instrument, but distinguishing strokes from radiant intracloud processes on a one-to-one basis is
52 still an unsolved problem.

53 Radio lightning measurements provide greater insights into the physical origin of
54 lightning signals, and one satellite flew with both optical and radio lightning sensors. We use
55 data collected by this FORTE satellite to investigate the link between physical lightning
56 processes (CG, in-cloud impulsive events, K-changes) and their optical signals. We confirm
57 many of the findings from previous studies, but also show that making inferences with optical
58 data alone can be problematic. Only optical and radio measurements, combined, provide a
59 complete picture of what is going on in the lightning flash and how the flash illuminates the
60 cloud.

61

62 **1 Introduction**

63 The Geostationary Lightning Mapper (GLM: Goodman et al., 2013) on NOAA's current-
64 generation Geostationary Operational Environmental Satellite (GOES) provides an
65 unprecedented continuous view of lightning activity across the Americas and a large fraction of
66 the Pacific Ocean. While ground-based long-range lightning detection networks report mainly
67 Cloud-to-Ground (CG) strokes (see Cummins and Murphy, 2009 for an overview of what
68 different types of networks can sense), space-based lightning imagers like GLM detect total
69 lightning - CG strokes plus intracloud (IC) discharges. Optical lightning imagers achieve total
70 lightning detection by measuring transient changes in cloud-top illumination. Any physical
71 process that lights up the cloud can be detected by GLM, not just powerful attachments to the
72 Earth's surface during CG strokes.

73 We have demonstrated that lightning imagers are capable of detecting weak optical
74 emissions from leader development and K-processes (Peterson et al., 2017a), including those that
75 are simultaneous with certain Transient Luminous Events (TLEs) such as gigantic jets (Boggs et
76 al., 2019). Moreover, because these instruments consist of pixelated Charge-Coupled Device
77 (CCD) arrays, they can be used to map the spatial evolution of individual lightning flashes over
78 time (Peterson et al., 2018) and identify truly exceptional lightning events (Peterson et al.,
79 2017b; Peterson et al., 2020a; Peterson and Kirkland, 2020; Peterson and Lay, 2020). These
80 observations have proven particularly useful for documenting lightning outside of the convective
81 core (Peterson and Liu, 2011; Peterson et al., 2020b) that tends to have a complex lateral
82 structure (Figures 6-8 in Peterson, 2019a).

83 GLM and similar instruments are a powerful tool for studying lightning physics on scales
84 that exceed the line-of-sight domains of ground-based Very High Frequency (VHF) band

85 Lightning Mapping Arrays (LMAs: Rison et al., 1999) and interferometer / optical whole sky
86 systems (Mazur et al., 1995, 1998). Space-based sensors further extend coverage to remote areas
87 of the world where ground-based measurements are impractical - including the open ocean.
88 There are two key limitations to space-based optical lightning measurements, however. First,
89 they provide limited information about the emissions source. Lightning imagers only measure
90 where clouds light up and by how much. Second, the lightning signals that make it to orbit have
91 been modified substantially by the intervening cloud layer between the source and the sensor
92 through scattering and absorption. The more exotic flash footprints measured by the Lightning
93 Imaging Sensor (LIS) and GLM suggest that there is as much information about the cloud scene
94 embedded within the lightning radiance data as there is about the flash (i.e., Peterson et al.,
95 2017a,b; Peterson, 2019b).

96 Due to the optical scattering effects in both space- and ground-based data, and a lack of
97 un-scattered optical measurements to serve as truth, there are large uncertainties inherent in any
98 attempt to infer a lightning discharge type on the basis of optical lightning data alone (Davis et
99 al., 2002; Koshak, 2010). For this reason, our recent analyses of optical phenomenology
100 (particularly Peterson and Rudlosky, 2019) have resisted making firm connections between
101 optical signatures and the physical processes that have traditionally been identified through
102 Radio-Frequency (RF) waveform analyses.

103 A comprehensive view of lightning from multiple types of measurements is required to
104 understand the evolution of lightning signals over the duration of the flash. In this study, we use
105 the wealth of coincident optical and VHF-band RF measurements provided by the Fast On-Orbit
106 Recording of Transient Events (FORTE) satellite to identify the physical origins of common
107 optical phenomena in the OTD, LIS and GLM datasets. We focus on lightning that produces

108 particularly large and radiant optical pulses that are consistent with return strokes from Koshak
109 (2010). Future work will examine other distinctive signatures including lateral flash
110 development.

111

112 **2 Data and Methodology**

113 The FORTE satellite was launched into Low Earth Orbit (LEO) in mid-1997. It had the
114 same 70° inclination angle as the MicroLab-1 satellite that hosted NASA's Optical Transient
115 Detector (OTD: Christian et al., 2003), but at a higher ~825 km orbit than OTD (710 km
116 altitude). Two key differences between FORTE and the NASA / NOAA instruments are: (1)
117 FORTE's coincident RF measurements that provide additional insights into transient lightning
118 emissions, and (2) FORTE being operated in campaign mode with instrument settings, collection
119 strategies, and trigger modes adjusted on-orbit. The coincident optical / RF data collected by
120 FORTE and its variety of operating modes create a niche for FORTE research that complements
121 lightning research with NASA's LIS and OTD, and NOAA's GLM instruments.

122 We use these combined optical / RF measurements to construct a new cluster feature
123 FORTE dataset similar to the LIS / OTD science datasets or the GLM operational data product.
124 This dataset (described in Section 2.3) encompasses all FORTE observations including the
125 various operating modes of the individual instruments. However, we only analyze one lightning
126 flash from this dataset in the present study. For this reason, we describe only the FORTE
127 instruments and operating modes relevant to this case in Sections 2.1 and 2.2. See Jacobson et al.
128 (1999) for a detailed description of the FORTE RF payloads and Suszcynsky et al. (2000, 2001)

129 for the optical payloads. Furthermore, Light (2020) provides a comprehensive review of the
130 FORTE mission and its novel scientific findings.

131 2.1 The FORTE Optical Lightning System

132 The FORTE Optical Lightning System (OLS) operated from late 1997 until early 2010
133 and consisted of two separate optical lightning detectors. The Lightning Locating System (LLS)
134 was a CCD lightning imager based on a modified version of the LIS/OTD design (Suszcynsky et
135 al., 2001). The key role of the LLS was geolocating lightning activity. The LLS had an 80°
136 square field of view across the CCD array that resulted in a ~10 km pixel size (similar to OTD).
137 The LLS frame rate was 405 FPS, which was lower than the nominal (500 FPS) and average on-
138 orbit (558 FPS) LIS frame rates (Bitzer and Christian, 2015). This design choice increased
139 lightning event detection while reducing event splitting between consecutive frames. The issue
140 of multiple lightning pulses contributing to events is not critical to FORTE, however, (as it was
141 for LIS / OTD) due to the availability of coincident high-speed instrumentation that could
142 identify individual pulses within a single LLS integration frame.

143 The second optical instrument was a photodiode detector (PDD) that provided broadband
144 (0.4 μm – 1.1 μm) fast (66,667 FPS) measurements of optical pulses from lightning over a large
145 field of view (Kirkland et al., 2001; Suszcynsky et al., 2001). The PDD record length and trigger
146 settings were reconfigured throughout the FORTE mission. The PDD data that we consider were
147 collected while the instrument was configured to have a record length of 1.92 ms and an
148 autonomous noise-riding amplitude threshold trigger. In the autonomous PDD trigger mode, the
149 optical signals must exceed the average background radiance for a specified duration (usually 5
150 samples or 75 μs) to trigger the instrument (Suszcynsky et al., 2000; Suszcynsky et al., 2001).

151 This limits triggering on energetic particle impacts, for example when the spacecraft was over
152 the South Atlantic Anomaly (SAA). There is also a finite number of PDD triggers that can be
153 captured on flash time scales. The maximum trigger count depends on the PDD configuration
154 and is usually a multiple of 10. During the time period where the flash of interest occurred, the
155 PDD was recording a maximum of 20 events per flash. This can cause flashes with substantial
156 in-cloud activity at the beginning of the flash to exhaust the available PDD triggers before the
157 return stroke occurs. We will show later on that this occurred with the flash of interest and, as a
158 result, the early development of the flash is well-resolved but the return stroke and later activity
159 is not captured by the PDD.

160 2.2 The FORTE Radio Frequency System

161 FORTE recorded RF transients from late 1997 until 2003. The FORTE RF system
162 consisted of two identical Log-Periodic Antennas (LPAs) mounted orthogonal to each other
163 along FORTE's 10-m nadir-pointing boom, and three broadband receivers that operated in the 26
164 to 300 MHz range (Jacobson et al., 1999; Suszcynsky et al., 2000; Shao and Jacobson, 2001;
165 Light et al., 2001a). The RF system had a 120° effective field of view that covered a ~6,000 km
166 diameter footprint on the surface of the Earth. Two of the three RF receivers comprise the TATR
167 payload that we use in this study. Each TATR receiver (designated TATR/A and TATR/B)
168 sampled one of the FORTE antennas at 50 megasamples per second (Shao and Jacobson, 2002).
169 The TATR receivers could be independently tuned to cover a desired 22 MHz subband. The
170 length of TATR records and the ratio of samples before and after the trigger were also
171 commandable. The TATR data that we consider had 800 μ s record lengths with 200 μ s of
172 pretrigger data, and TATR/A and TATR/B both set to record lowband (26 – 48 MHz) signals.

173 2.3 FORTE flash cluster data for combined optical / RF lightning measurements

174 Since LLS events are not clustered into features representing flashes or thunderstorms
175 during the original FORTE data processing, we generate our own LLS lightning cluster features
176 here. The techniques used to construct cluster feature data are described at length in the
177 LIS/OTD/GLM literature (Christian et al., 2000; Mach et al., 2007; Goodman et al., 2010). We
178 choose to adapt the clustering technique used with GLM (Goodman et al., 2010) to produce an
179 integrated FORTE lightning cluster feature dataset that establishes family links between LLS,
180 PDD and RF detections.

181 In the standard clustering hierarchy used by NASA and NOAA, the basic unit of
182 lightning detection is termed an “event.” On pixelated optical sensors such as LIS, OTD or
183 GLM, an event corresponds to a single pixel on the CCD array being triggered during a single 2-
184 ms integration frame. The FORTE literature uses a different definition for an LLS “event” that
185 permits detection across multiple integration frames. We use the NASA / NOAA convention
186 here and extract the triggered pixels from each frame in such cases to define unique events. We
187 also apply this event definition to PDD and RF detections by considering the entire FOV of these
188 instruments to be one “pixel” and the variable triggering intervals to be one “frame.” The
189 triggering interval is the minimum period of time until another trigger is possible, and includes
190 the record length plus any post-trigger dead time.

191 These modifications allow us to construct a general lightning cluster feature hierarchy
192 that can be applied to all FORTE instruments. The parent-child relationships between feature
193 levels and typical time domains are depicted in Figure 1. The data tree extends from
194 microsecond-scale “sample” features up through minute-scale “area” features that will be

195 defined below. We use this general template to fill out the full hierarchy of cluster features for
196 each FORTE instrument.

197 We start describing these features at the “event” level (Figure 1d) that is defined for all
198 FORTE instruments and represents a unique trigger. Moving up from the event level, the next
199 most complex feature is the “group.” Groups comprise contiguous portions of the instrument
200 FOV that produce events during a single frame. For this reason, they share the same panel as
201 events in Figure 1d. In the case of LLS, groups might contain multiple illuminated pixels whose
202 sides or corners touch on the CCD array. For the PDD and RF system (that contain just one
203 “pixel”), groups are identical to events.

204 Groups that occur close to one another in space and time are clustered into features
205 describing lightning flashes. Flash features (Figure 1b) are defined by applying a Weighted
206 Euclidian Distance (WED) model to the geolocated position and time displacements of groups
207 (Mach et al., 2007; Goodman et al., 2010). As with GLM, we use 16.5 km as the X and Y
208 distance thresholds and 330 ms as the time threshold. However, we choose to apply the WED
209 model to group centroids (as is done with LIS) rather than to group constituent event positions.
210 We do this to prevent overclustering - where highly-radiant pulses leading to very large groups
211 can merge all nearby concurrent lightning into a single flash.

212 The feature level between groups and flashes – “series” (Figure 1c) - requires flash
213 clustering in its derivation. Series features describe periods of sustained illumination from
214 lightning. Groups that (1) occur in consecutive frames or that have just one empty frame between
215 them and (2) are assigned to the same flash feature will be clustered into the same series feature.

216 Finally, area features (Figure 1a) describe thunderstorm snapshots during the FORTE
217 overpass. Areas are constructed by applying the group-to-flash clustering model (with no time
218 displacement term) to the flash centroid positions rather than the group centroid positions.

219 All of the features described above are computed for each FORTE instrument – LLS,
220 PDD, and the RF system. However, the PDD and RF system are both capable of constructing
221 features at finer time scales than events. PDD and RF records have a granularity on the order of
222 microseconds rather than milliseconds. We refer to the basic units of PDD and RF measurements
223 as “samples” (Figure 1f). We also define an intermediate “pulse” feature (Figure 1e) that is
224 comprised of multiple sequential samples within a single optical or RF event where the signal
225 exceeds the background average radiance (PDD) or power (TATR) by a specified threshold. For
226 this study, we specify that threshold to be one standard deviation above the mean background
227 value.

228 Certain feature levels are either not reported by some of the FORTE instruments or are
229 identical to other features in the clustering hierarchy for the same instrument. Table 1 lists the
230 features that are available to each instrument and shades the features that are most useful for
231 analyzing lightning activity. The features from each instrument (in each vertical column in Table
232 1) are linked via direct parent-child relationships. We also cross-link features from different
233 instruments by establishing “step-parent / step-child” relationships between higher-level features
234 from one instrument and lower-level features from another. For example, an LLS flash can be
235 the step-parent of a PDD event or RF pulse. The differing FOVs for the OLS (80°) and RF
236 system (120°) complicate the cross-linking because the RF system can detect events outside of
237 the LLS / PDD domain. To mitigate this issue, we adopt the Total Electron Content (TEC)
238 matching methodology from Jacobson et al., (1999) to screen for RF events that traverse a

239 different slant path through the ionosphere than the RF signals from the OLS flash in question. In
240 the following analyses, we will show all events that occurred in the same time frame as the flash
241 of interest and then exclude specific RF events that originated from elsewhere in the TATR
242 FOV.

243 **3 Results**

244 The goal of this study is to investigate the physical lightning processes that lead to
245 common optical signatures observed during LLS (and, by extension, LIS/OTD/GLM) flashes.
246 Associations between optical phenomena and physical processes are generally made by
247 observing such a process on the ground (i.e., continuing current from Bitzer, 2017 or gigantic
248 jets from Boggs et al., 2019) and then going back to the space-based lightning imager data to
249 determine (1) if it detected anything, and (2) whether the recorded signatures are consistent with
250 our understanding of the physics involved in such a process. If the instrument triggered and
251 produced a sufficiently unique optical signature, then the whole lightning imager record is
252 searched to find similar candidates for the process of interest.

253 We take the opposite approach here. We first look through our millions of FORTE
254 flashes to find cases that represent unique optical signatures, and then use the RF instrumentation
255 on FORTE to investigate what type of process produced the optical signals. This study focuses
256 on the very large and bright groups that may be return strokes in CG flashes (Koshak, 2010). A
257 case of oceanic lightning is identified that contains an exceptionally-radiant group that
258 illuminated a large cloud-top area – on the same scale as the extreme cases of LIS flashes
259 presented in Peterson et al. (2017b).

260 3.1 Overview of FORTE measurements during an oceanic CG flash on 10/13/1999

261 The selected case was observed over the Coral Sea northeast of Australia on 10/13/1999.
262 It produced 33 LLS groups clustered into 24 series over its 656 ms duration. Most groups were
263 dim optical pulses with the longest series lasting 19-ms. There were three particularly-radiant
264 groups that reached at least one standard deviation (σ) above the mean group energy. The
265 largest of these bright groups illuminated a cloud-top area of 3864 km^2 during a single LLS
266 frame. In total, the LLS observed 120 events associated with this flash while the PDD recorded
267 20 events (its maximum trigger count) and TATR recorded 73 events.

268 LLS Flash Extent Densities (FED: Lojou and Cummins, 2004) and trigger rates are
269 plotted in Figure 2 for the 15-minute window surrounding the flash. FED (Figure 2a) increments
270 once for every distinct lightning flash that illuminates a given grid point, regardless of how many
271 times that point is illuminated during the flash. It thus combines flash rate and flash extent into a
272 single gridded product. The FED plot indicates that the overall storm was neither extensive nor
273 organized. Lightning was broadly-scattered over the region and occurred at low rates. It is thus
274 likely that the optical footprint of the flash of interest was large (3864 km^2) because light was
275 able to illuminate nearby clouds, as we often see with LIS (Peterson and Liu, 2013; Peterson et
276 al., 2017a).

277 The trigger rate plot in Figure 2b counts the number of OLS, PDD, and TATR RF events
278 from 7.5 minutes before the flash to 7.5 minutes after the flash. Note that the time axis is not
279 linear, but accelerates near the zero line that represents the window encompassing the LLS flash
280 duration. Event rates are rather low before the flash at less than 10 per minute in most bins.
281 TATR and the PDD both trigger in the minute leading up to the flash, but there are no triggers of
282 any kind between 1 s and 0.33 s before its first LLS group. There are a few TATR triggers that
283 occur in the 1-second period after the flash, but none of these triggers have optical events

284 associated with them. Though these subsequent RF events could result from continued flash
285 activity that LLS does not resolve, we stop our analysis at LLS final light. With such low trigger
286 rates, we can be reasonably confident that our selected flash of interest is responsible for the
287 PDD and TATR events over the LLS flash duration, but we will verify this by comparing the
288 TEC measurements from the TATR events later on.

289 3.2 Evolution of optical signals from the flash

290 The evolution of LLS groups and events over the flash duration is shown in Figure 3. A
291 plan view is plotted in the central panel (Figure 3c) with total CCD pixel energy shown as a color
292 contour plot. Line segments depicting the spatial progression of groups from first light (dark
293 grey) to final light (light grey) are overlaid. The panel above the plan view (Figure 3a) shows the
294 longitude extent of each group in the flash, while the panel to the right (Figure 3d) shows latitude
295 extent. Figure 3b contains a histogram of group energy presented as a sigma level (i.e., the
296 number of standard deviations above or below the mean group energy for the flash). Finally, the
297 two panels below the plan view show timeseries of group area (Figure 3e) and group energy
298 (Figure 3f).

299 The two isolated events to the north of the flash footprint stand out as possible artifacts.
300 They both occur in the same LLS integration frame (364 ms after first LLS light), but are
301 clustered into separate flash features. This frame is important because it also contains the largest
302 and second-brightest group in the flash of interest (Figure 3e,f). Because these pixels do not light
303 up at any other point during the flash window, they may simply be reflections of the most radiant
304 pulse from the flash.

305 Figures 3e and f show that the LLS recorded 23 dim groups over the course of 350 ms
306 starting at LLS first light. This activity is then followed by a single series containing the two
307 largest and most energetic groups in the flash. After a lull for ~70 ms, the third bright group
308 occurs immediately following a low-energy group. Only two additional LLS groups are recorded
309 during the remaining 200 ms of the flash. Both final groups are brighter than the initial 23
310 groups, but they still have only ~10% of the radiance of the brightest group in the flash.

311 A first-order assessment of the optical flash without taking any other data into
312 consideration might be that the first groups describe in-cloud events during initial leader
313 development that culminate in peak optical emission at return stroke seawater attachment (near
314 362 ms in Figures 3e, f). The stroke lights up for two LLS frames due to either frame splitting
315 (i.e., the trigger time was at the end of the first group) or continuing current. There are two total
316 series that contain bright groups at the 1-sigma level, resulting in an optical multiplicity of two
317 and an interseries interval of 74 ms. The final LLS groups could be subsequent strokes or K-
318 changes. However, we cannot make any stronger inferences from the optical data, alone.

319 3.3 Combined optical and RF assessment of flash evolution

320 Fortunately, we do not have just the optical data to work with. The flash produced 73
321 TATR events over its duration that allow us to investigate what physical lightning processes are
322 occurring when light is detected by the LLS and PDD. Figure 4 shows timeseries of LLS groups,
323 and PDD and TATR events over the course of the flash. The time domain is expanded to include
324 the 200 ms before LLS first light in order to capture the initial RF events that did not have
325 coincident LLS or PDD triggers. Optical energy is shown in Figure 4a for LLS and Figure 4b for
326 PDD as a percent of the maximum group energy reported by each instrument. Optical energies

327 are plotted on a logarithmic scale to facilitate comparison with RF TATR event peak powers in
328 Figure 4c. After “dechirping” (correcting for ionospheric dispersion) and “prewhitening”
329 (suppressing narrowband carrier waves, for example from radio transmissions) the TATR
330 records returned for each event (these methods are summarized in Light et al., 2020), we
331 calculate the average power across the TATR band for each sample and then report the
332 maximum band-averaged RF power for all samples that are grandchildren of the event (see Table
333 1). Event peak powers are expressed in dB relative to the strongest RF emissions recorded over
334 the flash window (duration +/- 330 ms) in Figure 4c. All subsequent RF powers are reported
335 following this convention.

336 TATR pulse data are primarily used to classify the types of RF emissions from the flash
337 based on recognizable features in the TATR waveform data. The fractions of pulses in each 2-ms
338 window in Figure 4 that are isolated impulses (single peaks), single intracloud pulse pairs
339 (Trans-Ionospheric Pulse Pairs – TIPPs: Holden et al., 1995), pulse trains containing multiple
340 TIPPs, or diffuse / mixed (i.e., a diffuse pulse with impulsive peaks superimposed on the broad
341 waveform) are shown in Figure 4d. RF events that did not contain any perceptible pulses are
342 classified as single instances of “sustained featureless emission” per event.

343 TIPPs in VHF waveforms recorded from space result from in-cloud discharges where the
344 first peak that reaches the satellite comes from the direct line-of-sight detection of the RF pulse
345 and the second peak comes from the reflection of the pulse off the Earth’s surface (Jacobson et
346 al., 1999). For each TIPP case, we measure the time difference between the two pulses and use
347 the positions of the satellite and the nearest geolocated LLS group to estimate the altitude of the
348 in-cloud source. The altitudes of all TIPPs in the flash are plotted in Figure 4e. Finally, Figure 4f

349 integrates the LLS group radiance and TATR antenna response (in $V^2 m^{-2}$) over time to quantify
350 how the received optical and RF signals accumulated over the flash duration.

351 There are similarities between the overall optical evolution of the LLS flash shown in
352 Figure 3 and the evolution of the TATR flash shown in Figure 4c. The optical and RF flashes
353 both start out with a period of frequent weak triggers leading up to the most radiant LLS group.
354 We use TATR waveform analysis (Suszcynsky et al., 2000; Light et al., 2001) to conclude that
355 this energetic optical pulse was caused by a first negative return stroke. Optical and RF
356 timeseries from this event will be shown in Section 4.3.

357 The RF sources are primarily impulsive in-cloud events before the return stroke and then
358 diffuse K-change events afterwards (Figure 4d). There is a total of 103 impulsive in-cloud pulse
359 features in the 73 TATR events plus an additional 6 pulse features associated with the return
360 stroke and another 18 from diffuse K-changes. The impulsive in-cloud features are clustered into
361 two layers: a lower layer at 8 km altitude, and an upper layer at 12 km altitude. The TEC values
362 returned from the dechirping algorithm are nearly identical (65 ± 5 TECU) for all but two TATR
363 waveforms (not shown). Thus, 71 of the TATR events traversed the same slant path through the
364 ionosphere and came from the flash of interest. These two outlier events occurred at +14 ms and
365 +530 ms in Figure 4c and were the second and third most powerful RF pulses recorded during
366 the flash. Their reported TEC values were 110 ± 5 TECU and 140 ± 5 TECU (i.e., twice the TEC
367 experienced by the remaining RF signals – likely due to a relatively horizontal slant angle to the
368 satellite). We ignore these outlier events in subsequent analyses.

369 The TATR observations from the flash are consistent with ground-based VHF findings
370 from interferometer systems and LMA networks. Negative breakdowns in positive-polarity

371 charge regions radiate strongly in the VHF band measured by these ground-based systems, while
372 breakdowns in negative charge regions tend to be weaker. For this reason, Rison et al., (1999)
373 suggested that the relative difference in source counts between the upper and lower layers in a
374 bilevel flash is sufficient to determine the polarity of the breakdown and the charge regions
375 involved. In our case, most of the in-cloud sources preceding the return stroke come from the
376 upper layer (i.e., only 4 lower-layer sources occur from -200 ms to 250 ms). This suggests a
377 bilevel IC breakdown in a normal-polarity thunderstorm with a negative charge region at 8 km
378 altitude and a positive charge region at 12 km altitude.

379 While the period before the return stroke was characterized by frequent dim LLS groups,
380 the period following the return stroke only contained a small number of highly-radiant groups.
381 While most of the impulsive IC events in the flash came from the upper layer, no impulsive
382 sources were observed from this layer after +364 ms. Thus, the cessation of dim cloud pulses in
383 the LLS data coincides with the upper layer appearing to become cut off. This may be due to
384 increased attenuation experienced by the optical signals from the lower layer. When most RF
385 activity in our case is coming from the upper charge layer closer to the cloud top (first LLS light
386 until just before the return stroke) we have 41 RF events in forty 2-ms windows (Figure 4d)
387 compared to 24 total LLS groups. The trigger rate of LLS relative to TATR during this time
388 period is thus ~60%. For the period following the return stroke when the upper layer is quiet
389 (368 ms until the end of the LLS flash), there are 4 LLS groups compared to 14 TATR triggers in
390 11 2-ms windows. During this period, LLS triggers 28% of the time that TATR triggers, or in
391 ~36% of the 2-ms frames where TATR reports an event.

392 The optical and RF measurements of the flash also differ in their initial triggers. The LLS
393 flash begins with its lowest-radiance trigger at 0 ms. The PDD did not trigger alongside the LLS

394 until the radiance reaches around twice the radiance of this first LLS group (or 2% of the
395 maximum LLS group radiance for the flash). As a result, the start of the PDD flash is delayed by
396 40 ms relative to LLS. The TATR flash, on the other hand, precedes LLS first light by 136 ms
397 and begins with a single isolated impulsive in-cloud event that is followed by trains of cloud
398 pulses. This event was the most powerful RF event in the flash and waveform analysis indicates
399 that it resulted from a Narrow Bipolar Event (NBE). NBEs - also termed Compact Intracloud
400 Discharges (CIDs) - are quick in-cloud events that have comparable currents to return strokes
401 (~10 kA), but whose extents inferred from ground-based measurements are small – between 0.3
402 km and 1 km (Smith et al., 1999). NBEs are an example of “dark lightning” (Light and Jacobson,
403 2002; Jacobson et al., 2013) since they typically do not produce enough light (or perhaps no light
404 at all) to trigger optical instruments despite generating some of the most powerful natural RF
405 emissions on Earth.

406 We divide the hybrid CG flash into four phases based on its RF phenomenology: the
407 initial NBE (-136 ms), normal IC development following the NBE (-135 ms to 354 ms), the
408 return stroke (355 ms to 367 ms), and subsequent K-changes and in-cloud pulses following the
409 return stroke (368 ms to 800 ms). Each of these periods is discussed in depth below.

410 **4 Discussion**

411 **4.1 Initial NBE**

412 The flash of interest began with 6 TATR events in the 330 ms period leading up to first
413 LLS light (Figure 2b, Figure 4c). The first RF trigger occurred 136 ms before first LLS light and
414 was an isolated in-cloud event. This event was an example of the high-power impulsive in-cloud
415 lightning events discussed in the FORTE literature (Smith et al., 1999; Jacobson et al., 1999;

416 Light and Jacobson, 2002) that have been shown to be associated with NBEs (i.e., Rison et al.,
417 2016; Eack, 2004; Smith et al., 1999). These events are among the most powerful VHF lightning
418 sources (LeVine, 1980) and occur at altitudes ranging from 6 km to 15 km (Light and Jacobson,
419 2002). See Rison et al. (2016) for a review on NBEs.

420 NBEs / CIDs can occur in relative isolation (Smith et al., 1999), or as the first VHF pulse
421 that sets off a normal IC flash (Rison et al., 1999). A National Lightning Detection Network
422 (NLDN: Cummins et al., 1998) analysis of CID events suggests that 73% are isolated while 24%
423 occur before, during, or after “normal” lightning, and the remaining 4% occur in pairs separated
424 by no more than 200 ms (Nag et al., 2010).

425 The NBE at -136 ms occurred near the lower charge later at 9 km altitude and began a
426 period of normal in-cloud activity that lasted for 400 ms. This TATR event was the strongest RF
427 emitter recorded during the flash - even compared to the return stroke. It contributed 9% of the
428 total received RF energy for the flash (Figure 4f) despite being an impulsive event. Even with
429 this strong RF emission, it was not optically bright enough to trigger the LLS or PDD - which is
430 typical of NBEs (Light and Jacobson, 2002).

431

432 4.2 Normal IC activity

433 The normal IC activity following the NBE produced regular TATR triggers with an
434 average interval of 9 ms between successive events. All but 4 triggers from -135 ms to +354 ms
435 (just before the return stroke) were low-power TIPPes and pulse pair trains from normal IC
436 breakdowns. This IC phase was the most active period during the flash and contained 22 out of

437 33 LLS groups, all 20 PPD events, and 48 out of 73 TATR events. The PDD exhausted its
438 available triggers within the first 300 ms of the LLS flash. LLS optical emissions during this
439 period were between 1% and 10% of the peak LLS radiance during the return stroke. In total, the
440 IC phase of the flash contributed 22% of the received RF energy and 23% of the optical LLS
441 radiance from the flash. This apparent agreement between optical and RF is probably
442 coincidental since TATR triggered regularly for 52 ms before first LLS light, and the
443 accumulation of optical energy is relatively piecemeal compared to the nearly constant rate at
444 which RF signals accumulated after the CID.

445 The first 100 ms of the flash is shown in LLS evolution plot in Figure 5. Figure 5 is
446 identical to Figure 3, but with OLS group (greyscale by group number) and PDD sample (blue)
447 energy depicted on a logarithmic scale in panel (e), and TATR sample RF power (blue) shown in
448 panel (f). There were 4 LLS groups in the first 100 ms of the LLS flash. The two that consisted
449 of 2 events also triggered the PDD, while the 2 single-event groups did not. The first group in the
450 flash was also the dimmest at just 1% the maximum group energy. PDD triggering on multi-pixel
451 LLS groups continued for the next 112 ms in the flash duration (not shown).

452 The optical and RF events during the first 212 ms of the LLS flash are all isolated in time
453 with TATR and the PDD waveforms describing impulsive sources. Figure 6 shows the next
454 period of the flash that included sustained optical emission over an extended period of time. The
455 longest LLS series in the flash lasted 19 ms (8 LLS frames) starting at +247 ms. However, this
456 LLS series is part of a longer period of consecutive PDD triggers that started at +220 ms and
457 ended at +278 ms. Despite the dead time between records (approximately equal to the record
458 length) and impulsive peaks notable in the blue PDD light curve in Figure 6e, the flash appears
459 to have been generating sustained optical emission the whole time as the LLS groups / events

460 started to expand westward in Figure 6c. The LLS groups during this period were generally dim
461 ($< 1\sigma$ in Figure 6b), and periods where PDD triggered but LLS did not suggest that the sources
462 were not spatially concentrated enough to trigger individual LLS pixels.

463

464 4.3 Return stroke

465 Optical and RF signals during the 12-ms window encompassing the return stroke are
466 shown in Figure 7. Starting with TATR trigger at +358 ms, the flash produced the constantly-
467 strengthening sustained featureless emission associated with stepped leader development ahead
468 of a first negative return stroke (Light et al., 2001a) over a 4.5 ms period. Seawater attachment
469 occurred at +362 ms and the strong narrow VHF peak was accompanied by the most radiant LLS
470 group in the flash.

471 The VHF emissions surrounding the return stroke accounted for 21% of the overall
472 TATR antenna response, but the optical emissions accounted for 58% of the total flash energy
473 recorded by LLS (Figure 4f). The evolution plot for this period is shown in in Figure 7a-d. The
474 optical emissions are divided into 6 groups in two LLS frames. Because multiple groups occur in
475 each of these two frames, the groups become overlaid in Figure 7e, resulting in only three
476 distinct entries being notable in the group radiance timeseries.

477 The two largest groups both have radiances above the 3-sigma level in Figure 7b. Lines
478 are not drawn connecting these groups to the preceding group-level structure of the flash in
479 Figure 7c due to the large distances separating them from the nearest preceding group, but their
480 positions can still be noted in Figure 7a and d. Two of these groups occur within the flash

481 footprint in Figure 7c, while the remaining two occur north of the flash. Because these pixels did
482 not light up at any other time, we speculate that they are reflections rather than coincident
483 lightning activity.

484 The two isolated groups that occur within the flash footprint are distinct because only a
485 portion of the 4751 km² flash footprint is illuminated during each LLS frame. The western half
486 of the flash is illuminated in the first frame along with an isolated event to the east (Figure 7a),
487 and then the eastern portion of the flash footprint is illuminated in the second frame along with
488 an isolated western event. This second bright group is less radiant than the first, but has the
489 largest group area at 3864 km² (81% of the overall flash footprint area).

490 Because the eastern and western portions of the flash footprint are illuminated in separate
491 LLS frames, there are pixels – even near the flash center – that are illuminated during one group
492 and not the other. Since no subsequent groups are observed, we can conclude that the LLS glint
493 filter was not activated and that the flash likely did not have prolonged continuing current.
494 However, there are also pixels within the flash footprint that were not illuminated during either
495 frame associated with the return stroke. The three black pixels in Figure 7c form a hole in the
496 middle of an otherwise-contiguous feature on the LLS CCD array. We have noted this behavior
497 before with LIS flashes (Figure 1 in Peterson and Liu, 2013 is one example) where coincident
498 radar data show that such optical holes correspond to dense convective cells embedded in the
499 flash footprint that seem to block radiance from reaching the satellite. Dark pixels causing
500 “holes” in otherwise contiguous flash footprints during intense low-altitude processes provides
501 further evidence that clouds modify the optical signals recorded from orbit – even to the point of
502 preventing detection. The pixels corresponding to the hole were illuminated during earlier

503 periods of the flash dominated by high-altitude IC pulses (including in Figure 6c), and thus the
504 hole is not observed in Figure 3c.

505

506 4.4 Post-RS K-changes and IC pulses

507 The final phase of the flash describes the K-changes and in-cloud pulses following the
508 return stroke. In-cloud activity was limited to the lower (8 km) charge layer and dominated by K-
509 processes. Four LLS groups were detected, but no subsequent strokes were identified in the
510 TATR waveform data. This final period provided the remaining 19% of optical energy in the
511 flash and the final 47% of the total TATR response. These TATR signals were supplied by
512 diffuse VHF events that produced broad RF pulses. Three such TATR events in the 75-ms period
513 following the return stroke did not trigger the LLS. However, a particularly strong and long-
514 lasting K-change occurred at +440 ms that was followed by strong optical emission. The VHF
515 and optical measurements from this period are shown in Figure 8. The TATR antenna response
516 integrated over the waveform for this trigger was 24% greater than the return stroke, and it
517 produced the third-brightest LLS group. As with the in-cloud pulses preceding the return stroke,
518 there was no hole in this group – the K-change illuminated the entire convective core of the
519 parent thunderstorm.

520 This group was also the only group outside of the series encompassing the return stroke
521 to reach the 1-sigma radiance level and thus advance the optical multiplicity. The fact that it was
522 caused by a K-change rather than a subsequent stroke justifies our previous aversion to drawing
523 parallels between the traditional RF-based multiplicity parameter and our new optical
524 multiplicity parameter (Peterson and Rudlosky, 2019). The optical multiplicity is simply a

525 measure of how many times a flash lights up the clouds above a reference value based on weak
526 cloud pulses, and can capture radiant processes other than strokes.

527

528 **5 Conclusion**

529 Coincident optical and RF measurements from the FORTE satellite are used to examine
530 the joint evolution of an oceanic CG lightning flash. The first signals received during the flash
531 window (330 ms before first light until 330 ms after final light) included an apparent NBE (-136
532 ms) that set off a period of regular RF triggering on impulsive in-cloud events. This period of
533 normal IC activity lasted for 490 ms until the beginning of stepped leader activity ahead of the
534 return stroke. Cloud pulses were clustered into an upper layer at 12 km altitude and a lower layer
535 at 8 km altitude, consistent with a bilevel hybrid CG flash. The relative frequency of RF
536 triggering in the two layers suggests that the storm had a normal charge structure and the CG
537 flash was of negative polarity. Cloud pulses are noted in only the lower layer following the
538 return stroke, and are accompanied by diffuse RF emissions from K-changes.

539 The optical flash began 52 ms after the NBE. The initial IC phase of the flash produced
540 22 of its 30 optical groups. These groups were generally weak, varying between 1% and 10% of
541 the peak group energy for the flash, and contributed 23% of the total flash radiance. There were
542 no such weak triggers during the 4.5 ms of stepped leader activity leading up to the return stroke.
543 The most radiant optical groups occurred upon attachment over the course of 2 LLS integration
544 frames (~5 ms). The bright group in the first frame was the most energetic in the flash, while the
545 bright group in the second frame was dimmer with a larger area. The next LLS group occurred
546 74 ms later during a K-change event. No subsequent strokes were observed in the VHF
547 waveform data.

548 These results demonstrate how coincident space-based optical and RF measurements can
549 be used to construct a comprehensive view of lightning that is more informed than the
550 perspectives from either measurement type in isolation. RF measurements confirm the physical
551 origin of optical signals and document events that are too optically dim to be detected from
552 space. Optical measurements provide geolocation information for RF events and highlight
553 periods of sustained current flow in both CG and IC phases of the flash. Our analyses support the
554 idea that large and bright groups result from return strokes, but also that radiant processes like K-
555 changes similarly stand out above the baseline emissions from the flash. While the value of
556 instruments such as GLM for investigating lightning physics in flashes across the hemisphere
557 cannot be overstated, there is a significant benefit to taking a data fusion approach between
558 available optical and RF measurements to prevent mis-associations and gain a clearer picture of
559 what is going on.

560

561 **Acknowledgments**

562 Los Alamos National Laboratory is operated by Triad National Security, LLC, under contract
563 number 89233218CNA000001. The data presented in this study are located at Peterson (2020).

564

565 **References**

- 566 Bitzer, P. M., 2017: Global distribution and properties of continuing current in lightning, *J. Geophys. Res. Atmos.*,
567 **122**, 1033–1041, doi:10.1002/2016JD025532
- 568 Bitzer, P.M. and H.J. Christian, 2015: Timing Uncertainty of the Lightning Imaging Sensor. *J. Atmos. Oceanic*
569 *Technol.*, **32**, 453–460, <https://doi.org/10.1175/JTECH-D-13-00177.1>

- 570 Boggs, L. D., N. Liu, M. Peterson, S. Lazarus, M. Splitt, F. Lucena, A. Nag, and H. Rassoul, 2019: First
571 observations of gigantic jets from geostationary orbit. *Geophys. Res. Lett.*, **46**,
572 <https://doi.org/10.1029/2019GL082278>
- 573 Budden, K. G., 1985: The Propagation of Radio Waves. *Cambridge Univ. Press*, New York
- 574 Cecil, D. J., D. E. Buechler, and R. J. Blakeslee, 2014: Gridded lightning climatology from TRMM-LIS and OTD:
575 Dataset description. *Atmos. Res.*, **1350136**, 404-414
- 576 Christian, H. J., R. J. Blakeslee, S. J. Goodman, and D. M. Mach (Eds.), 2000: Algorithm Theoretical Basis
577 Document (ATBD) for the Lightning Imaging Sensor (LIS), NASA/Marshall Space Flight Center,
578 Alabama. (Available as <http://eosps.gsfc.nasa.gov/atbd/listables.html>, posted 1 Feb. 2000)
- 579 Christian, H. J., R. J. Blakeslee, D. J. Boccippio, W. L. Boeck, D. E. Buechler, K. T. Driscoll, S. J. Goodman, J. M.
580 Hall, W. J. Koshak, D. M. Mach, and M. F. Stewart, 2003: Global frequency and distribution of lightning
581 as observed from space by the Optical Transient Detector. *J. Geophys. Res.*, **108**(D1), ACL-4.
- 582 Cummins, K. L., M. J. Murphy, E. A. Bardo, W. L. Hiscox, R. B. Pyle, and A. E. Pifer, 1998: A combined
583 TOA/MDF technology upgrade of the U.S. National Lightning Detection Network. *J. Geophys. Res.*, **103**,
584 9035–9044
- 585 K. L. Cummins and M. J. Murphy, 2009: An Overview of Lightning Locating Systems: History, Techniques, and
586 Data Uses, With an In-Depth Look at the U.S. NLDN, *IEEE Trans. on Electromag. Compat.*, **51**, 3, pp.
587 499-518, doi: 10.1109/TEMC.2009.2023450.
- 588 Eack, K. B. (2004), Electrical characteristics of narrow bipolar events, *Geophys. Res. Lett.*, **31**, L20102,
589 doi:[10.1029/2004GL021117](https://doi.org/10.1029/2004GL021117).
- 590 Goodman, S. J., D. Mach, W. J. Koshak, and R. J. Blakeslee, 2010: GLM Lightning Cluster-Filter Algorithm
591 (LCFA) Algorithm Theoretical Basis Document (ATBD). NOAA NESDIS Center for Satellite
592 Applications and Research. (Available as [https://www.goes-](https://www.goes-r.gov/products/ATBDs/baseline/Lightning_v2.0_no_color.pdf)
593 [r.gov/products/ATBDs/baseline/Lightning_v2.0_no_color.pdf](https://www.goes-r.gov/products/ATBDs/baseline/Lightning_v2.0_no_color.pdf), posted 24 Sept. 2010)
- 594 Goodman, S. J., R. J. Blakeslee, W. J. Koshak, D. Mach, J. Bailey, D. Buechler, L. Carey, C. Schultz, M. Bateman,
595 E. McCaul Jr., and G. Stano, 2013: The GOES-R geostationary lightning mapper (GLM). *J. Atmos. Res.*,
596 **125-126**, 34-49

- 597 Holden, D. N., C. P. Munson, and J. C. Devenport, 1995: Satellite observations of transionospheric pulse pairs,
598 *Geophys. Res. Lett.*, **22**, 889–892
- 599 Jacobson, A. R., S. O. Knox, R., Franz, and D. C. Enemark, 1999: FORTE observations of lightning radio-frequency
600 signatures: Capabilities and basic results. *Radio Sci.*, **34** (2), 337– 354, doi:10.1029/1998RS900043
- 601 Jacobson, A. R., K. L. Cummins, M. Carter, P. Klingner, D. Roussel-Dupré, and S. O. Knox, 2000: FORTE radio-
602 frequency observations of lightning strokes detected by the National Lightning Detection Network. *J.*
603 *Geophys. Res.*, **105** (D12), 15653– 15662, doi:10.1029/2000JD900103
- 604 Jacobson, A. R., and X.-M. Shao, 2002: FORTE satellite observations of very narrow radiofrequency pulses
605 associated with the initiation of negative cloud-to-ground lightning strokes. *J. Geophys. Res.*, **107** (D22),
606 4661, doi:10.1029/2001JD001542
- 607 Jacobson, A. R., T. E. L. and Light, 2003: Bimodal radio frequency pulse distribution of intracloud-lightning signals
608 recorded by the FORTE satellite. *J. Geophys. Res.*, **108**, 4266, doi:10.1029/2002JD002613, D9
- 609 Jacobson, A. R., Light, T. E. L., Hamlin, T., & Nemzek, R. (2013). Joint radio and optical observations of the most
610 radio-powerful intracloud lightning discharges. *Annales Geophysicae (09927689)*, *31*(3).JPL, 2019: Global
611 Ionospheric Maps. Accessed 7 May 2019, <https://iono.jpl.nasa.gov/gim.html>
- 612 Koshak, W. J., 2010: Optical characteristics of OTD flashes and the implications for flash-type discrimination. *J.*
613 *Atmos. Oceanic. Technol.*, **27**, 1,822 – 1,838
- 614 Le Vine, D. M. (1980). Sources of the strongest RF radiation from lightning. *Journal of Geophysical Research:*
615 *Oceans*, *85*(C7), 4091-4095.
- 616 Light, T. E., D. M. Suszcynsky, and A. R. Jacobson, 2001a: Coincident radio frequency and optical emissions from
617 lightning, observed with the FORTE satellite. *J. Geophys. Res.*, **106** (D22), 28223– 28231,
618 doi:10.1029/2001JD000727
- 619 Light, T. E., D. M. Suszcynsky, M. W. Kirkland, and A. R. Jacobson, 2001: Simulations of lightning optical
620 waveforms as seen through clouds by satellites. *J. Geophys. Res.*, **106** (D15), 17103– 17114,
621 doi:10.1029/2001JD900051
- 622 Light, T. E. L., and A. R. Jacobson, 2002: Characteristics of impulsive VHF lightning signals observed by the
623 FORTE satellite. *J. Geophys. Res.*, **107** (D24), 4756, doi:10.1029/2001JD001585

- 624 Lojou, J.-Y., K. L. Cummins, 2004: On the representation of two- and three-dimensional total lightning information.
625 In Preprints, Conference on Meteorological Applications of Lightning Data (pp. Paper 2.4, AMS Annual
626 Meeting, San Diego, CA, USA)
- 627 Mach, D. M., H. J. Christian, R. J. Blackeslee, D. J. Boccippio, S. J. Goodman, and W. L. Boeck, 2007:
628 Performance assessment of the Optical Transient Detector and Lightning Imaging Sensor. *J. Geophys. Res.*,
629 **112**, D09210
- 630 Massey, S. R., S. O. Knox, R. C. Franz, D. N. Holden, and C. T. Rhodes, 1998: Measurements of transionospheric
631 radio propagation parameters using the FORTE satellite. *Radio Sci.*, **33**, 1739–1753
- 632 Mazur, V., P. R. Krehbiel, and X.-M. and Shao, 1995: Correlated high-speed video and radio interferometric
633 observations of a cloud-to-ground lightning flash. *J. Geophys. Res.*, **100** (D12), 25731– 25753,
634 doi:10.1029/95JD02364
- 635 Mazur, V., X.-M. Shao, and P. R. Krehbiel, 1998: “Spider” lightning in intracloud and positive cloud-to-ground
636 flashes. *J. Geophys. Res.*, **103** (D16), 19811– 19822, doi:10.1029/98JD02003
- 637 Nag, A., V. A. Rakov, D. Tsalikis, and J. A. Cramer, 2010: On phenomenology of compact intracloud lightning
638 discharges. *J. Geophys. Res.*, **115**, D14115, doi:10.1029/2009JD012957
- 639 Peterson, M., 2019a: Research applications for the Geostationary Lightning Mapper operational lightning flash data
640 product. *J. Geophys. Res.*, **124**, 10205– 10231. <https://doi.org/10.1029/2019JD031054>
- 641 Peterson, M., 2019b: Using lightning flashes to image thunderclouds. *J. Geophys. Res.*, **124**, 10175– 10185.
642 <https://doi.org/10.1029/2019JD031055>
- 643 Peterson, M., 2020, CIERRA-FORTE Flash Cluster Data, <https://doi.org/10.7910/DVN/63FWWU>, Harvard
644 Dataverse, DRAFT VERSION
- 645 Peterson, M. J. and C. Liu, 2011: Global statistics of lightning in anvil and stratiform regions over the tropics and
646 subtropics observed by TRMM, *J. Geophys. Res.*, **116**, D23, doi: 10.1029/2011JD015908
- 647 Peterson, M. J. and C. Liu, 2013: Characteristics of lightning flashes with exceptional illuminated areas, durations,
648 and optical powers and surrounding storm properties in the tropics and inner subtropics, *J. Geophys. Res.*,
649 **118**, 11,727-11,740, doi: 10.1002/jgrd.50715
- 650 Peterson, M. J., W. Deierling, C. Liu, D. Mach, C. Kalb, 2017a: The properties of optical lightning flashes and the
651 clouds they illuminate. *J. Geophys. Res. Atmos.*, **122**, 423–442, doi:10.1002/2016JD025312

- 652 Peterson, M. J., S. Rudlosky, and W. Deierling, 2017b: The evolution and structure of extreme optical lightning
653 flashes. *J. Geophys. Res. Atmos.*, **122**, doi: 10.1002/2017JD026855
- 654 Peterson, M., S. Rudlosky, and W. Deierling, 2018: Mapping the Lateral Development of Lightning Flashes from
655 Orbit. *J. Geophys. Res. Atmos.*, **123**, 9674– 9687. <https://doi.org/10.1029/2018JD028583>
- 656 Peterson, M., S. Rudlosky, 2019: The time evolution of optical lightning flashes. *J. Geophys. Res.*, **124**, 333– 349.
657 <https://doi.org/10.1029/2018JD028741>
- 658 Peterson, M. J., Lang, T. J., Bruning, E. C., Albrecht, R., Blakeslee, R. J., Lyons, W. A., et al., 2020a: New World
659 Meteorological Organization certified megaflash lightning extremes for flash distance (709 km) and
660 duration (16.73 s) recorded from space. *Geophys. Res. Lett.*, **47**, e2020GL088888.
661 <https://doi.org/10.1029/2020GL088888>
- 662 Peterson, M., S. Rudlosky, and D. Zhang, 2020b: Thunderstorm Cloud-Type Classification from Space-Based
663 Lightning Imagers. *Mon. Wea. Rev.*, **148**, 1891–1898, <https://doi.org/10.1175/MWR-D-19-0365.1>.
- 664 Rison, W., R.J. Thomas, P.R. Krehbiel, T. Hamlin, and J. Harlin, 1999: A GPS-based three-dimensional lightning
665 mapping system: initial observations in central New Mexico. *Geophys. Res. Lett.*, **26**, 23, 3573-3576.
- 666 Shao, X.-M., 2018: Broadband RF Interferometric Mapping and Polarization (BIMAP) observations of Mini-
667 Discharges in thunderstorms. AGU Fall Meeting 2018, Washington, DC, Amer. Geophys. Union.
668 <https://agu.confex.com/agu/fm18/meetingapp.cgi/Paper/422277>
- 669 Shao, X.-M., and A. R. Jacobson, 2001: Polarization observations of broadband VHF signals by the FORTE
670 satellite. *Radio Sci.*, **36** (6), 1573– 1589, doi:10.1029/2000RS002600
- 671 Shao, X.-M., and A. R. Jacobson, 2002: Polarization observations of lightning-produced VHF emissions by the
672 FORTE satellite, *J. Geophys. Res.*, **107** (D20), 4430, doi:10.1029/2001JD001018
- 673 Smith, D. A., X.-M. Shao, D. N. Holden, C. T. Rhodes, M. Brook, P. R. Krehbiel, M. Stanley, W. Rison, and R. J.
674 Thomas, 1999: A distinct class of isolated intracloud lightning discharges and their associated radio
675 emissions. *J. Geophys. Res.*, **104** (D4), 4189– 4212, doi:10.1029/1998JD200045
- 676 Suszcynsky, D. M., M. W. Kirkland, A. R., Jacobson, R. C. Franz, S. O. Knox, J. L. L. Guillen, and J. L. Green,
677 2000: FORTE observations of simultaneous VHF and optical emissions from lightning: Basic
678 phenomenology. *J. Geophys. Res.*, **105** (D2), 2191– 2201, doi:10.1029/1999JD900993

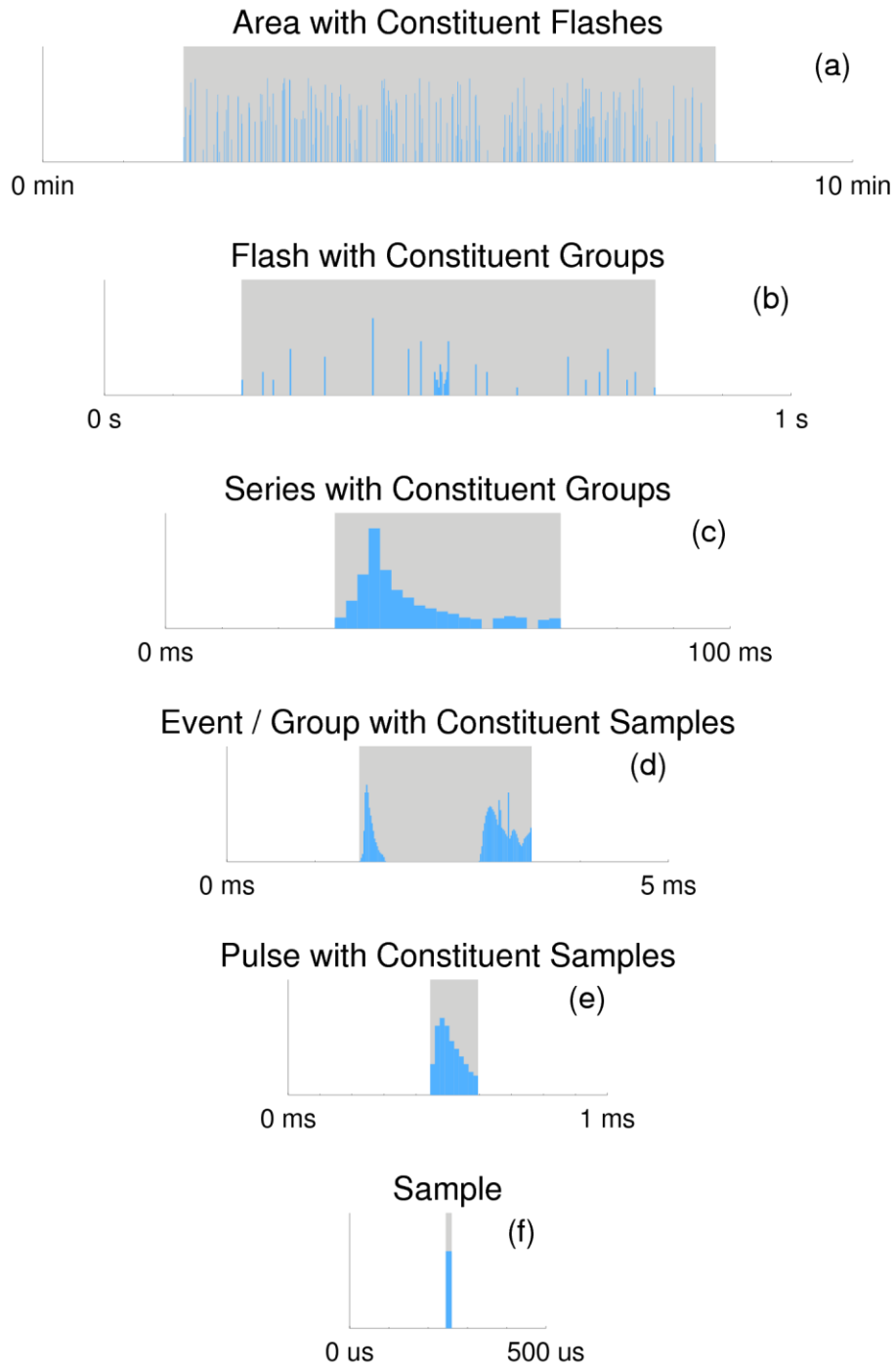
679 Suszcynsky, D. M., T. E. Light, S., Davis, J. L., Green, J. L. L. Guillen, and W. Myre, 2001: Coordinated
680 observations of optical lightning from space using the FORTE photodiode detector and CCD imager. *J.*
681 *Geophys. Res.*, **106** (D16), 17897– 17906, doi:10.1029/2001JD900199
682

683 **Table 1.** A tabular representation of the parallel tree data structures that describe lightning cluster features for each
 684 FORTE instrument. Useful features for analyzing lightning flashes are shaded. Note the vertical offsets due to
 685 relevant time scales varying by instrument
 686

Time Scale	OLS		RFS	
	LLS	PDD	TATR	HUMR
10^3 s	VIEWTIME	VIEWTIME	VIEWTIME	VIEWTIME
10^2 s	AREA BACKGROUND	AREA BACKGROUND	AREA BACKGROUND	AREA BACKGROUND
10^1 s	FLASH	FLASH	FLASH	FLASH
10^0 s	SERIES	SERIES	SERIES	SERIES
10^{-1} s	GROUP / EVENT	GROUP / EVENT	GROUP / EVENT	GROUP / EVENT
10^{-2} s		PULSE	PULSE	PULSE
10^{-3} s		SAMPLE	SAMPLE	SAMPLE
10^{-4} s				
10^{-5} s				
10^{-6} s				
10^{-7} s				

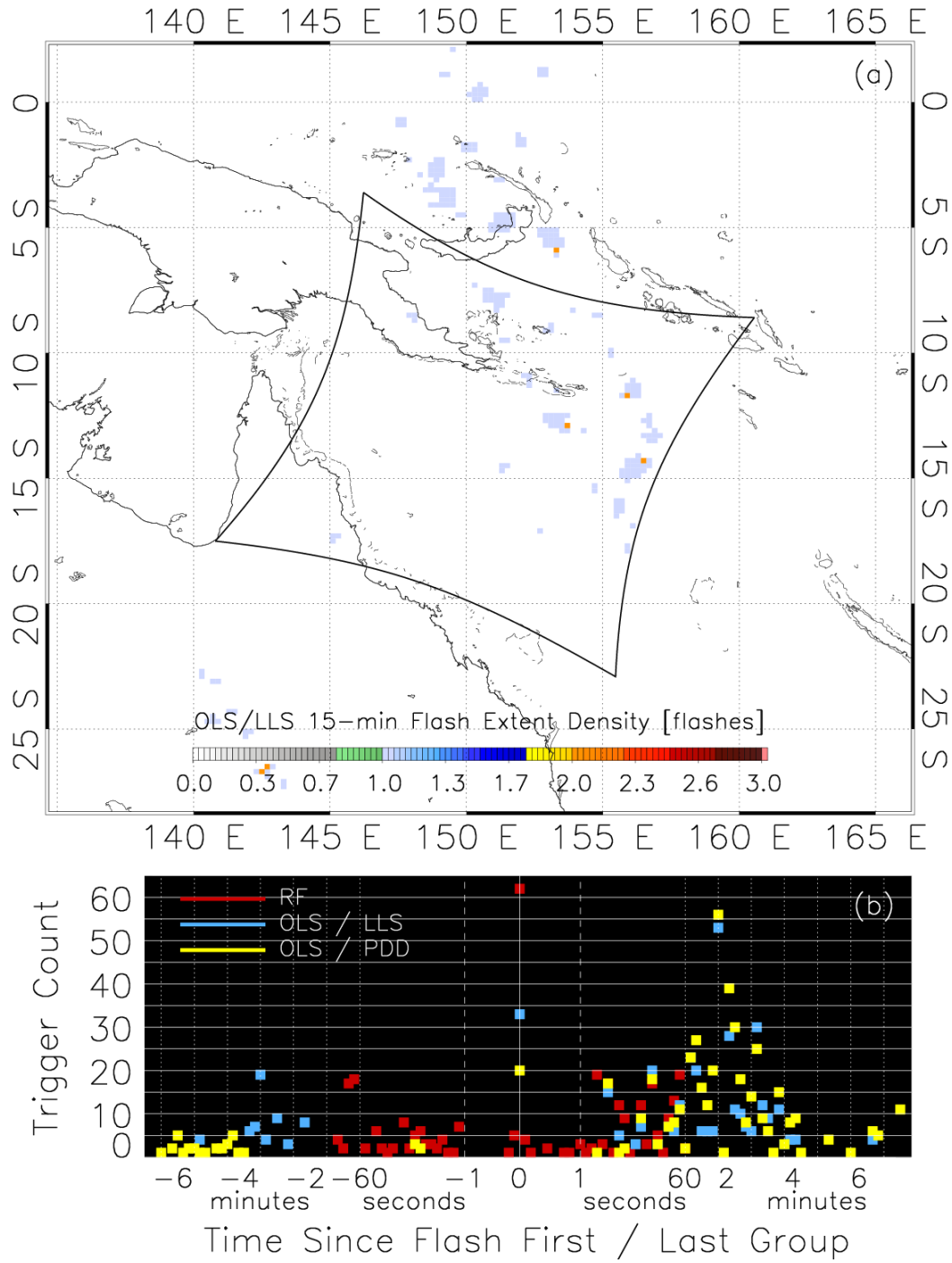
687
 688
 689

690



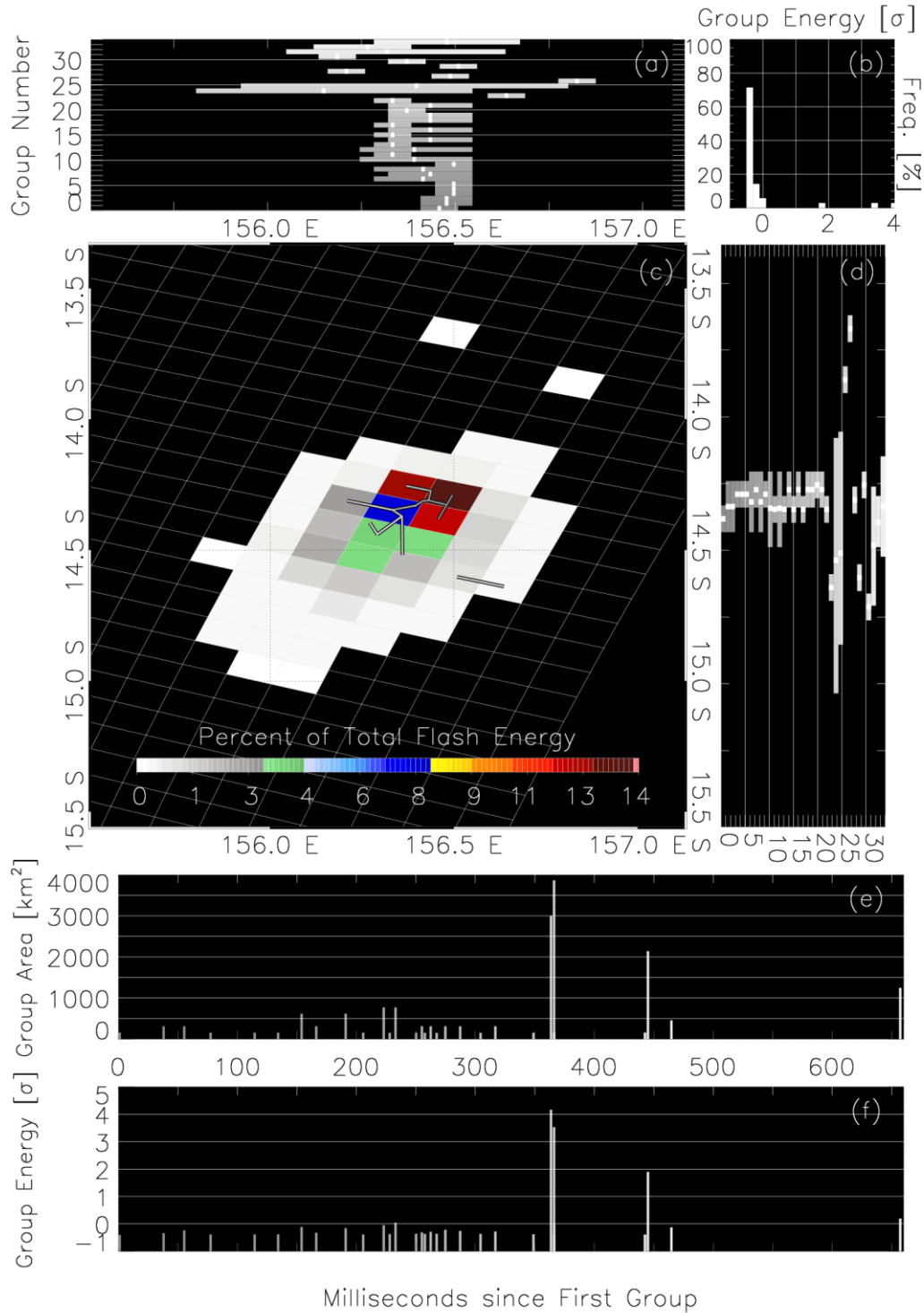
691
 692
 693
 694
 695
 696
 697
 698

Figure 1. The general lightning cluster feature hierarchy used for all FORTE instruments and the time domain associated with each feature. Features are the parents of features above them on the diagram and children of the features below them. The grey boxes show the domain of the current feature at each level while constituent lower-level features are shaded blue.



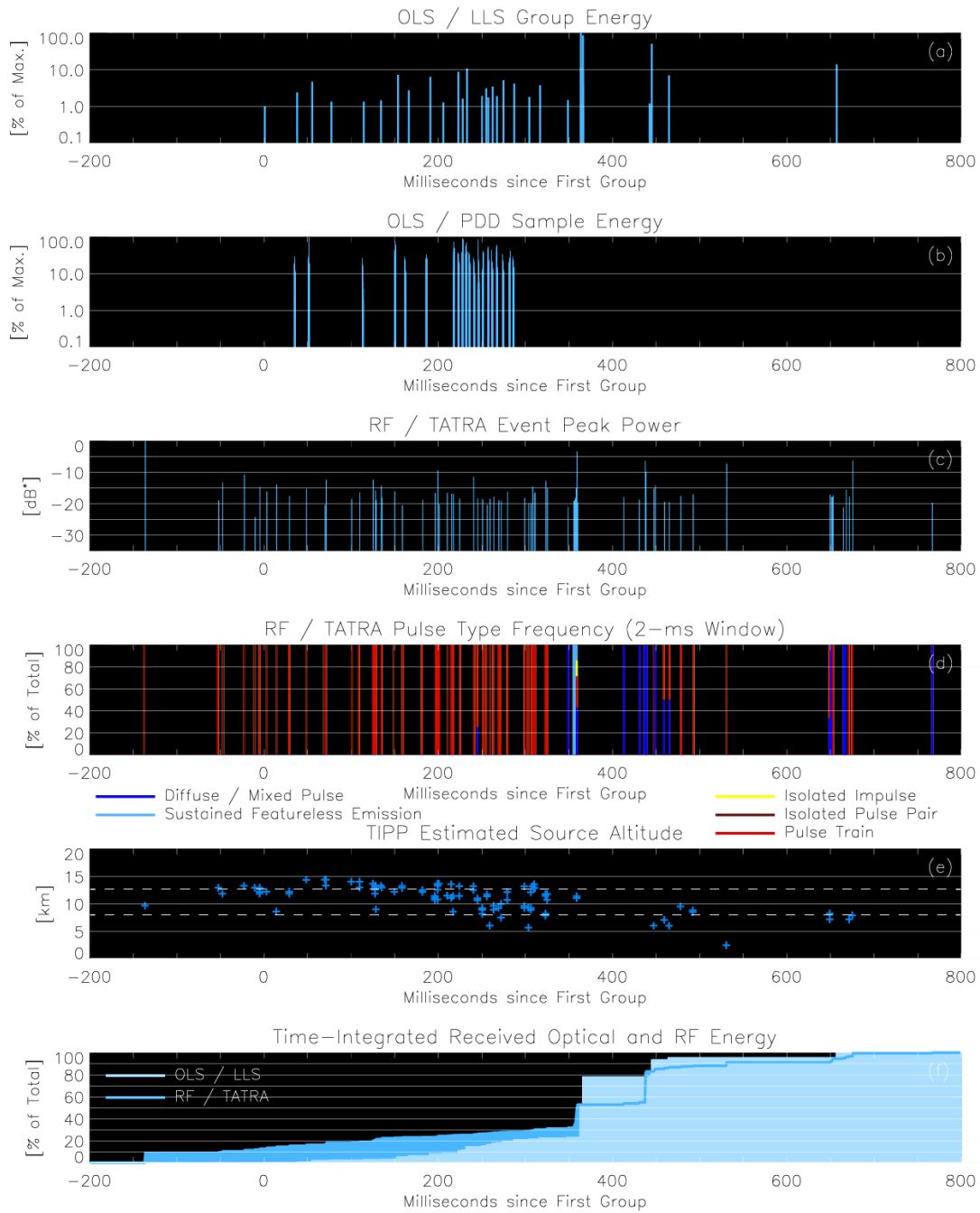
699
700
701
702
703
704
705

Figure 2. FORTE LLS lightning activity close to the flash of interest. (a) FED across the LLS FOV and (b) optical and RF trigger rates during the 15-minute window surrounding the flash. Because lightning was infrequent across the FORTE FOV during the flash window, signals from other flashes are unlikely. (Should you mark on the map the interested flash?)



706
707
708
709
710
711
712

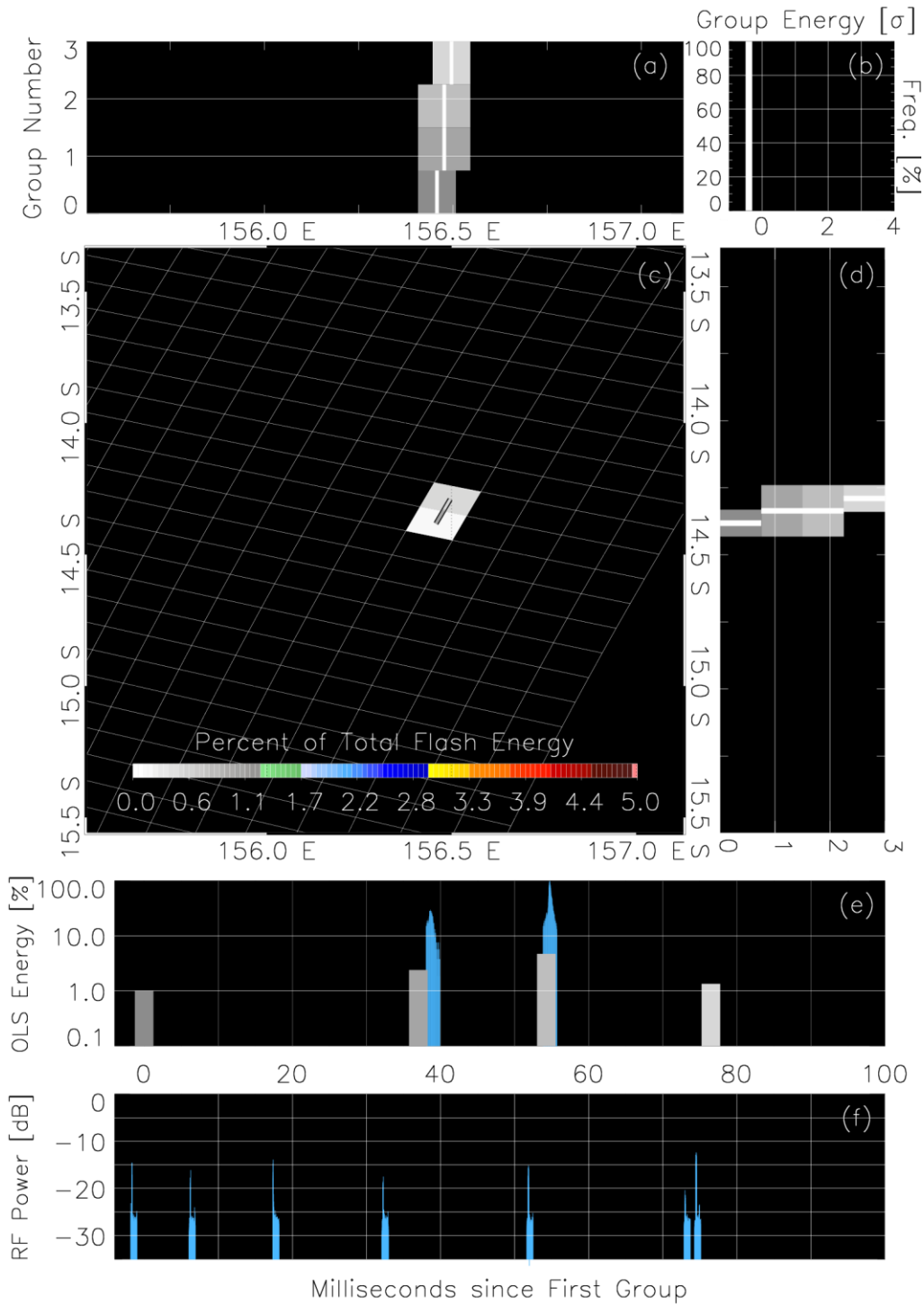
Figure 3. Evolution plot for the LLS flash. (a) group extent by longitude, (b) group energy distribution, (c) plan view of flash energy (color contour) and group extent (line segments), (d) group extent by latitude, (e) timeseries of group area, and (f) timeseries of group energy. Group energies are expressed as a sigma level relative to the average group energy in the flash. The greyscale in all plots represents the sequential group index.



713
714
715
716
717
718
719
720

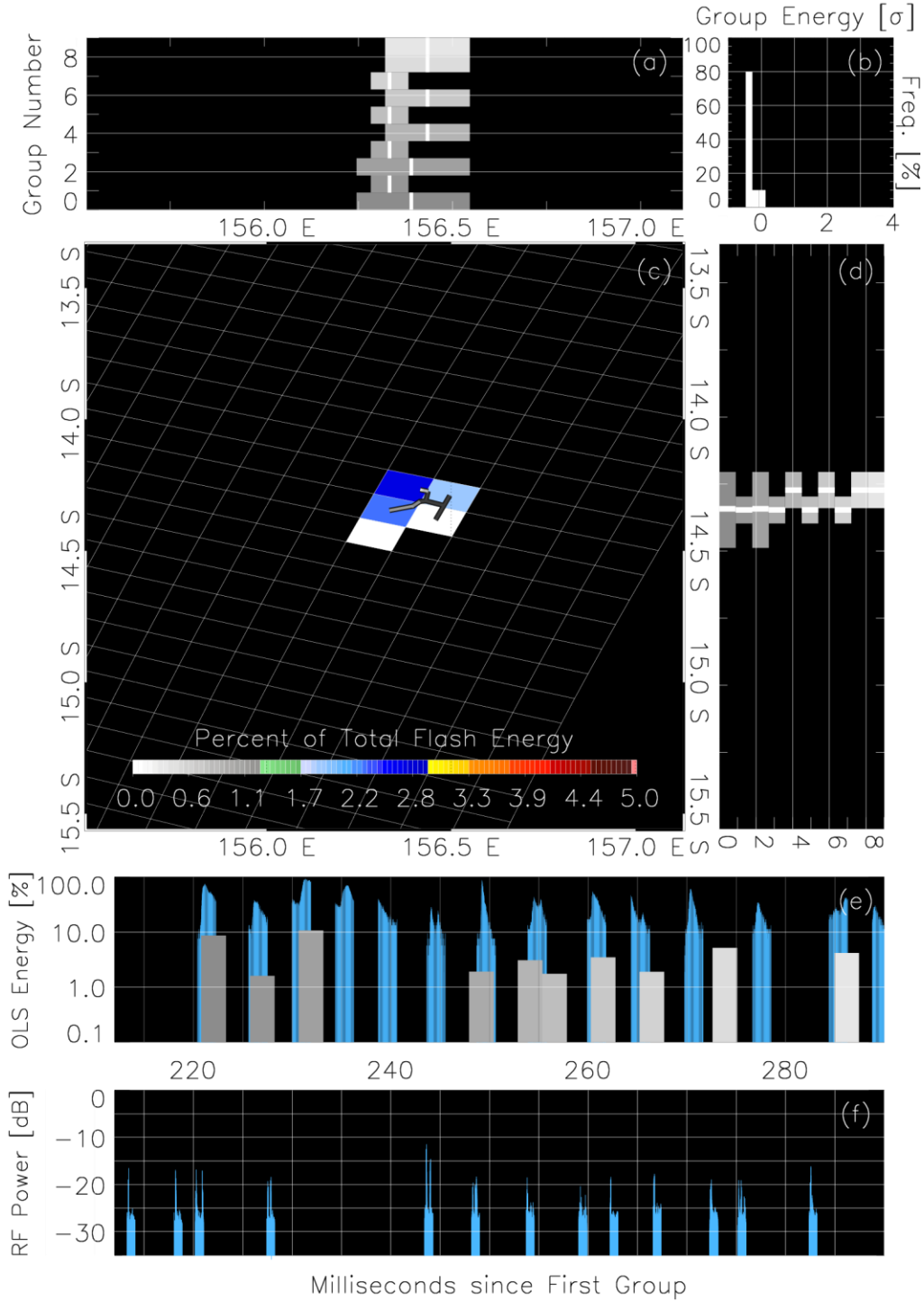
Figure 4. Timeseries showing the combined optical / RF evolution of the flash. (a) LLS and (b) PDD optical energies. (c) TATR RF power (* signifies relative to the overall peak RF power during the flash window). (d) TATR pulse classification shown as the frequency of each pulse type in a 2-ms window. (e) estimated altitude of in-cloud (TIPP) sources. (f) time-integrated optical and RF energies over the flash duration

721



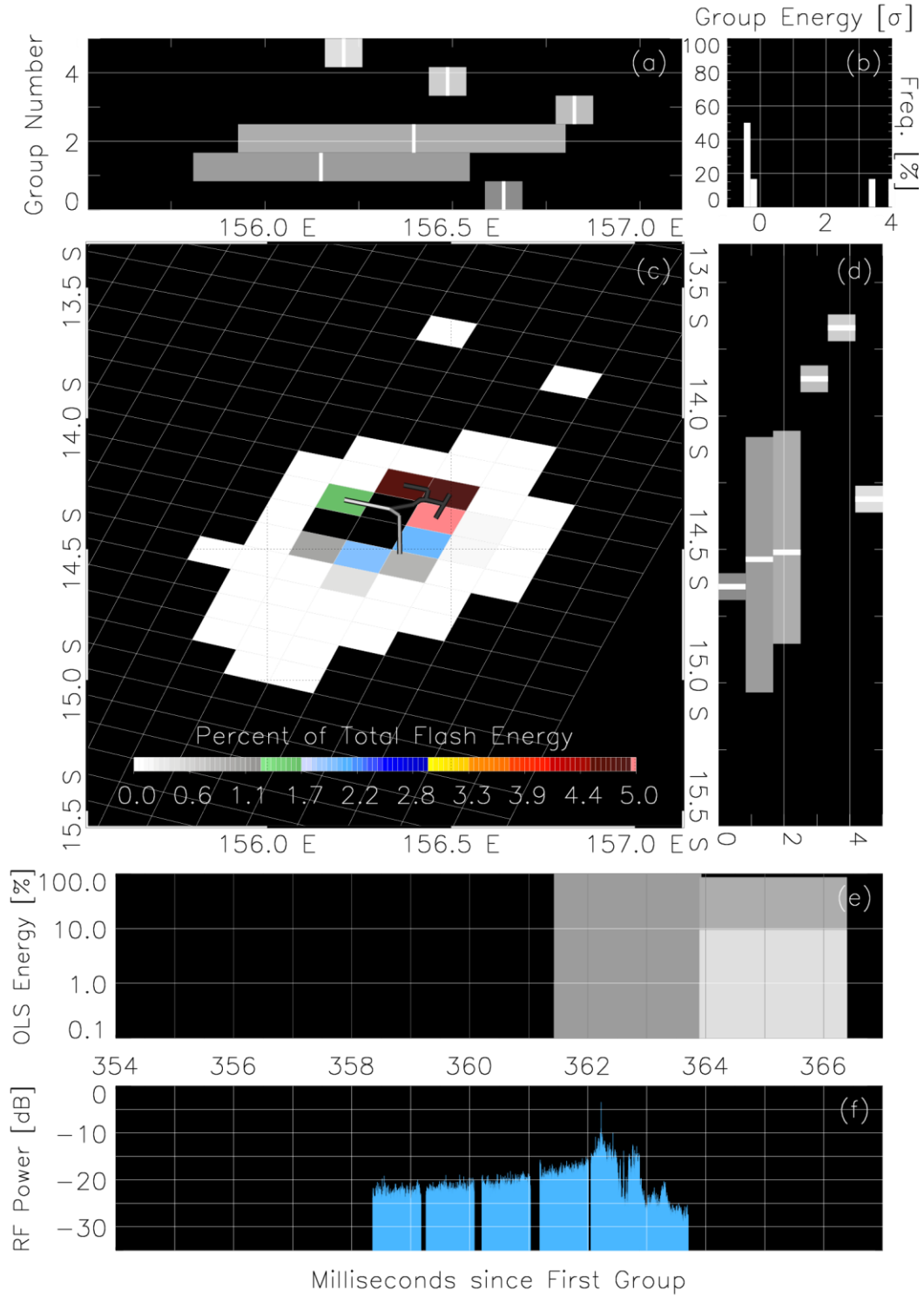
722
723
724
725
726
727

Figure 5. Evolution plot for the first 100 ms of optical triggers in the flash. Identical to Figure 3, but with LLS group area replaced by TATR RF power in (f) and PDD data plotted blue in (e).



728
729
730
731
732

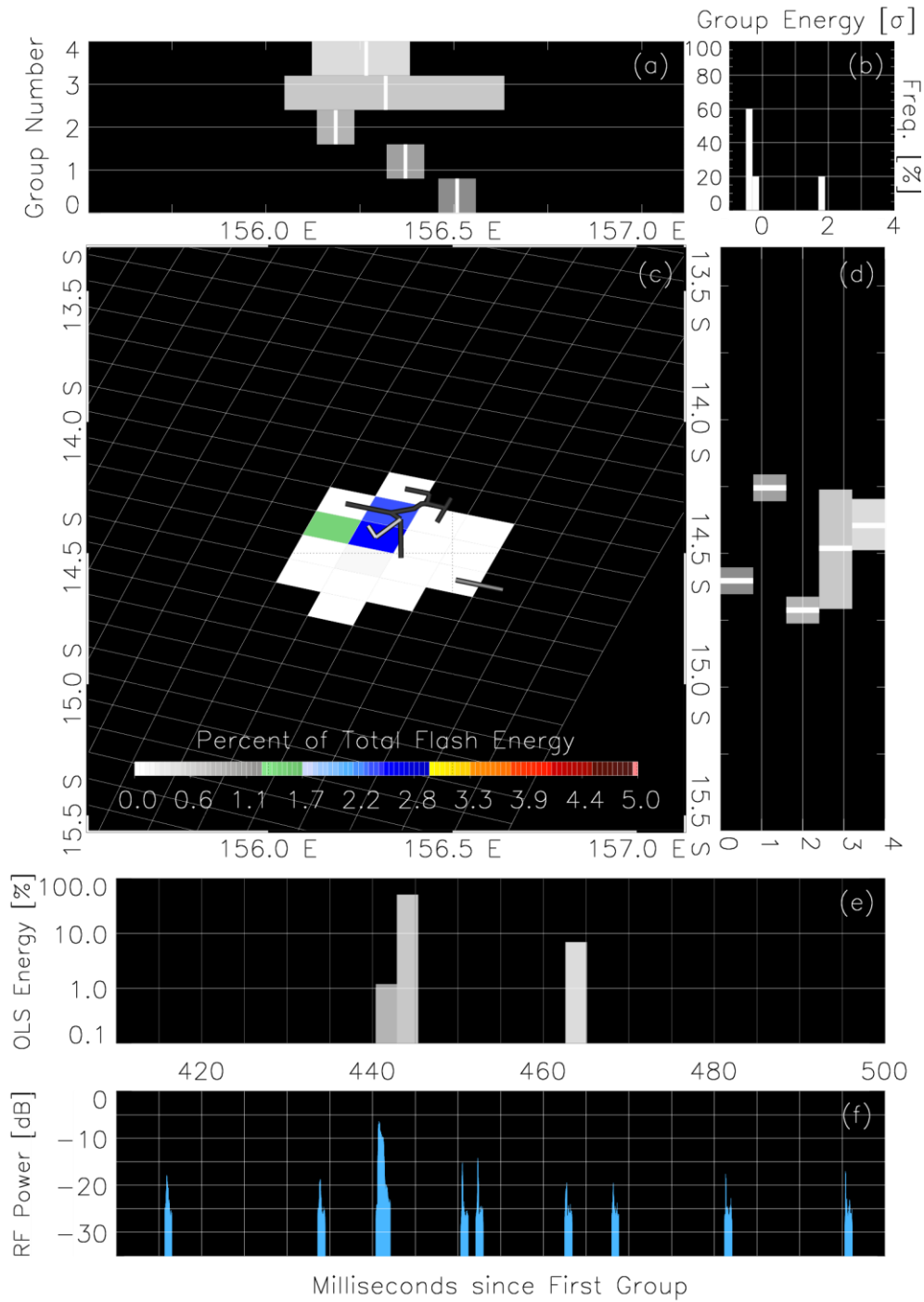
Figure 6. Same as Figure 5, but for the period 212 ms – 290 ms that encompasses a long-lasting PDD series.



733
734
735
736

Figure 7. Same as Figure 5, but for the period 354 ms – 367 ms that contains the return stroke.

737



738

739

740 **Figure 8.** Same as Figure 5, but for the period 410 ms – 500 ms that contains the final bright LLS group.

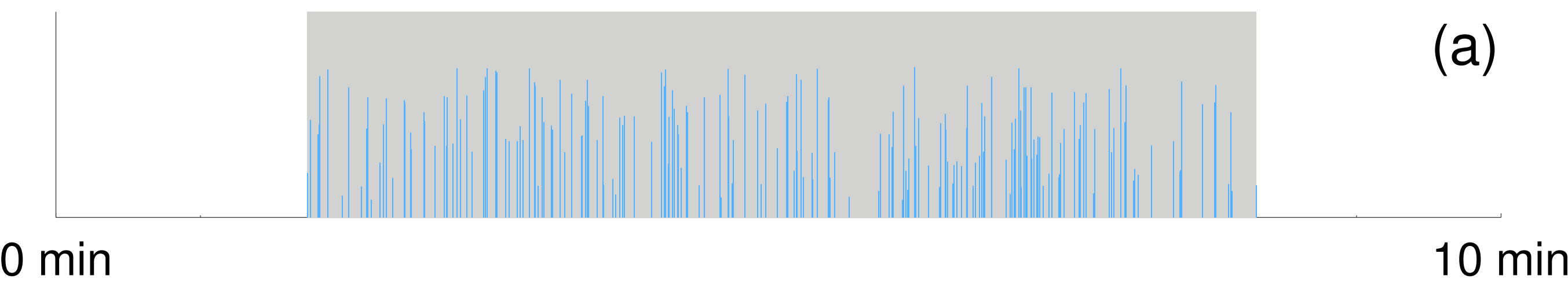
741

742

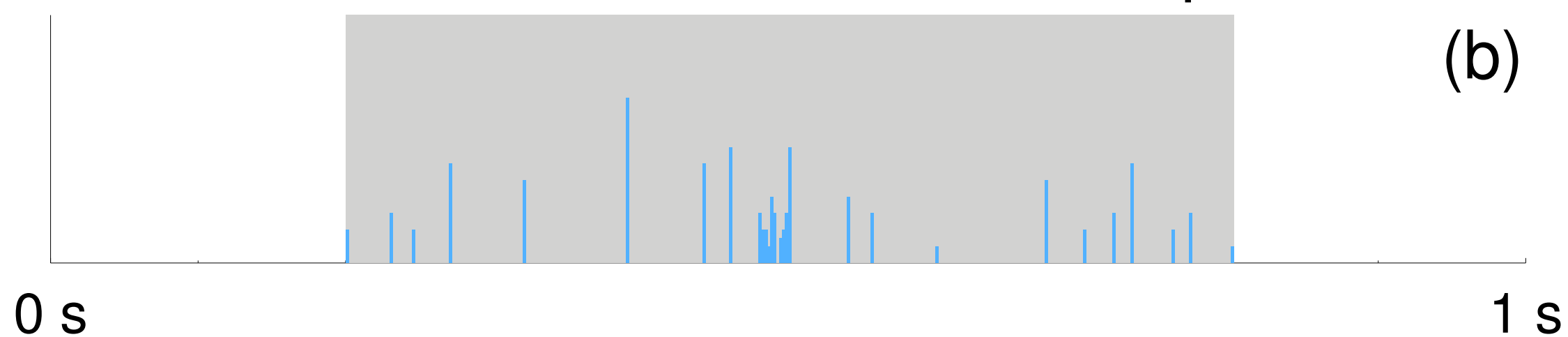
743

Figure 1.

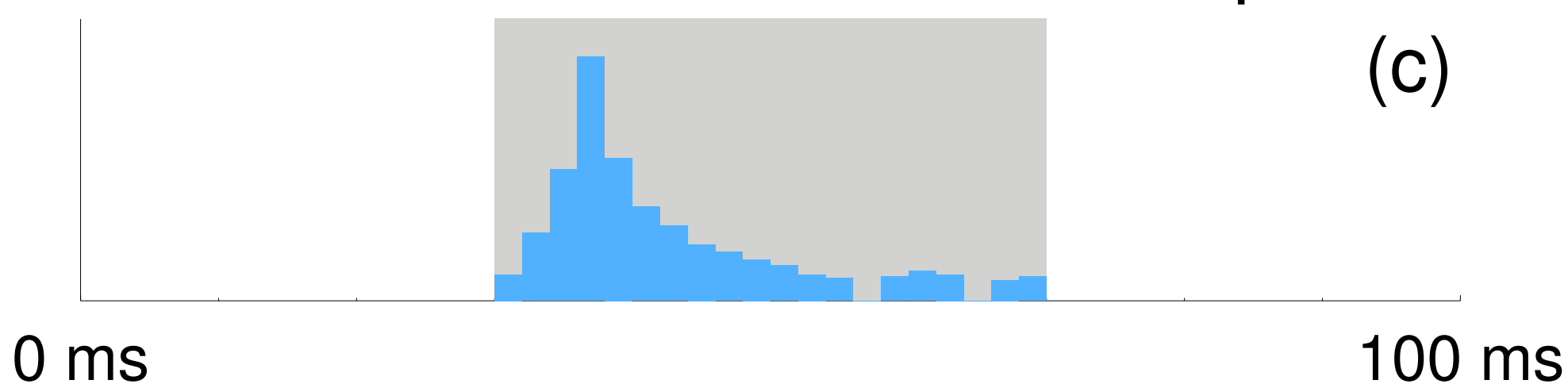
Area with Constituent Flashes



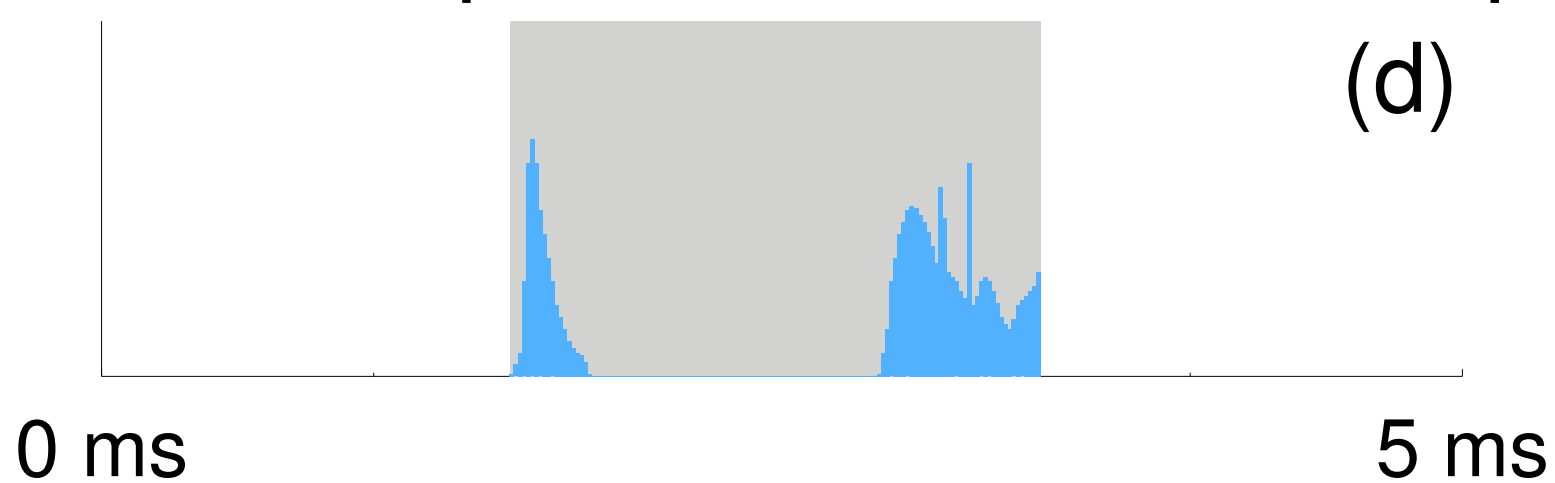
Flash with Constituent Groups



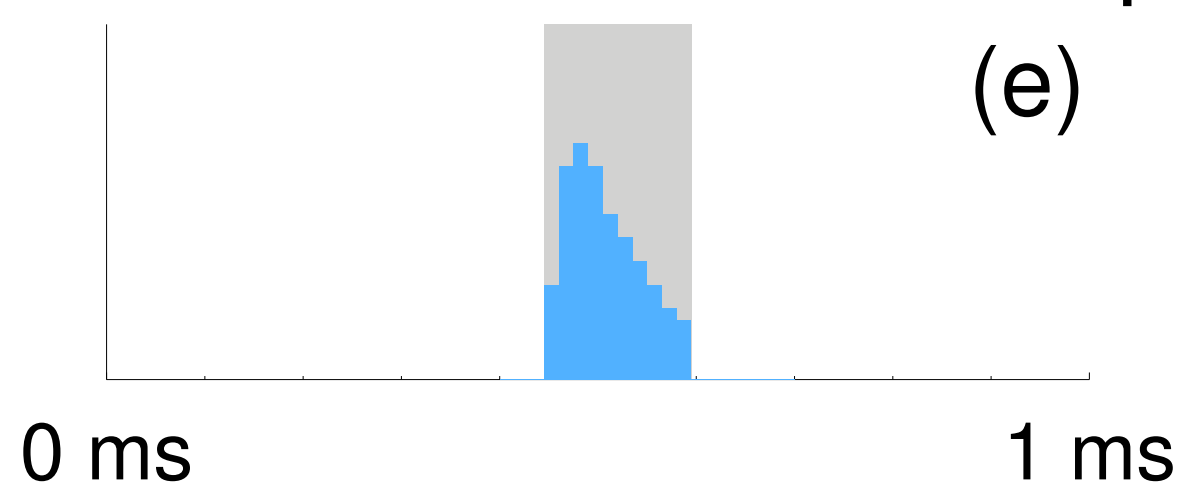
Series with Constituent Groups



Event / Group with Constituent Samples



Pulse with Constituent Samples



Sample

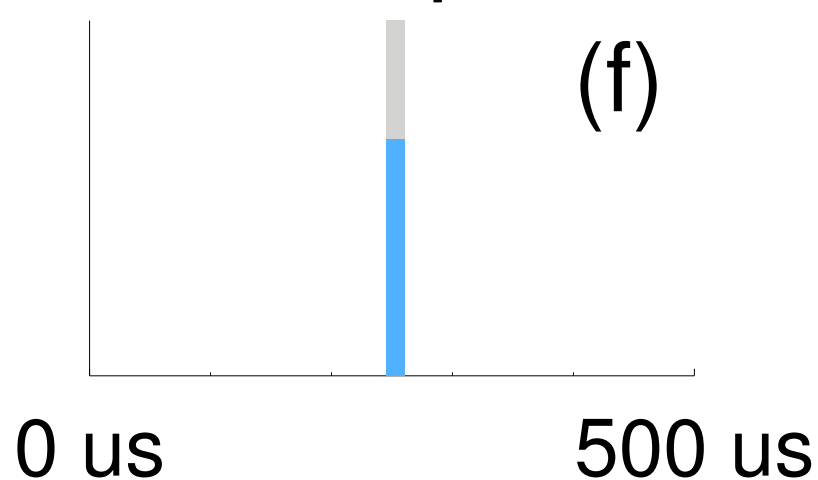


Figure 2.

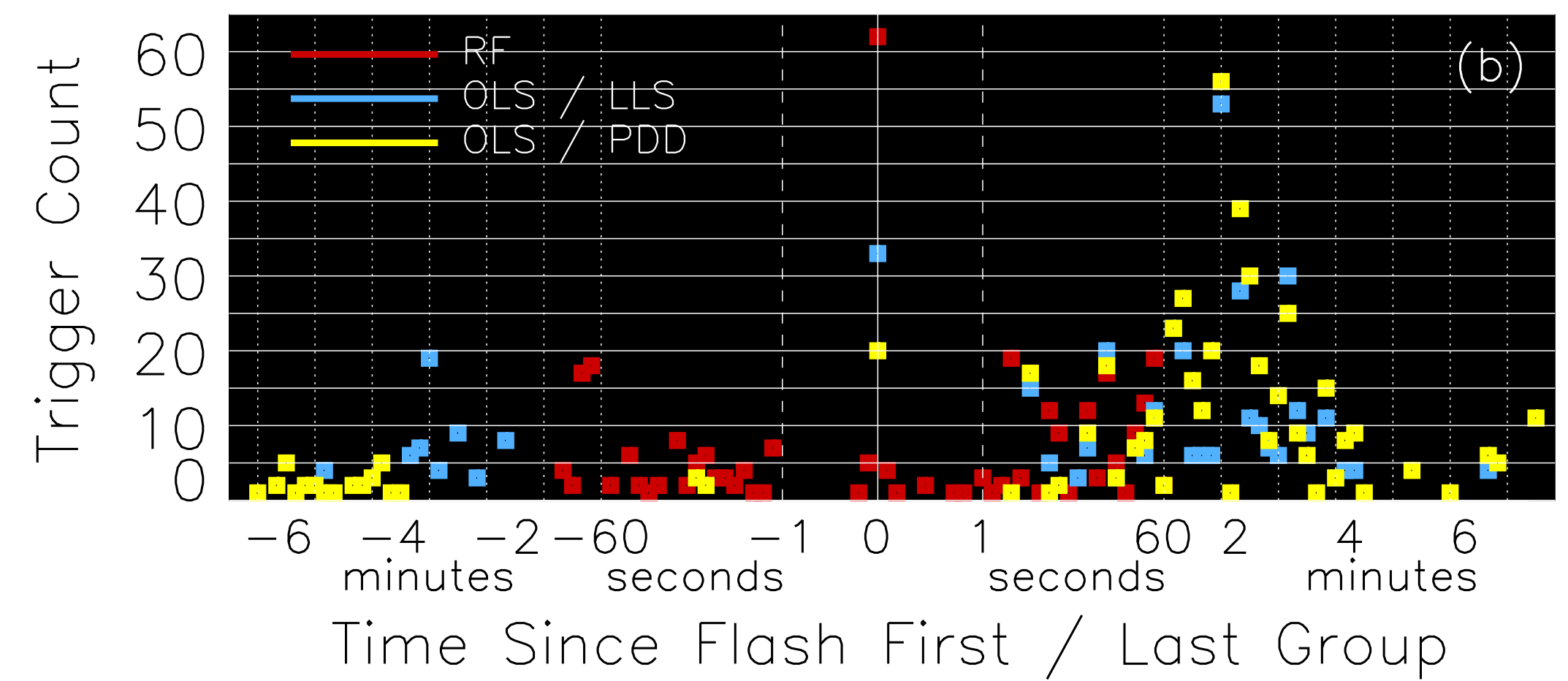
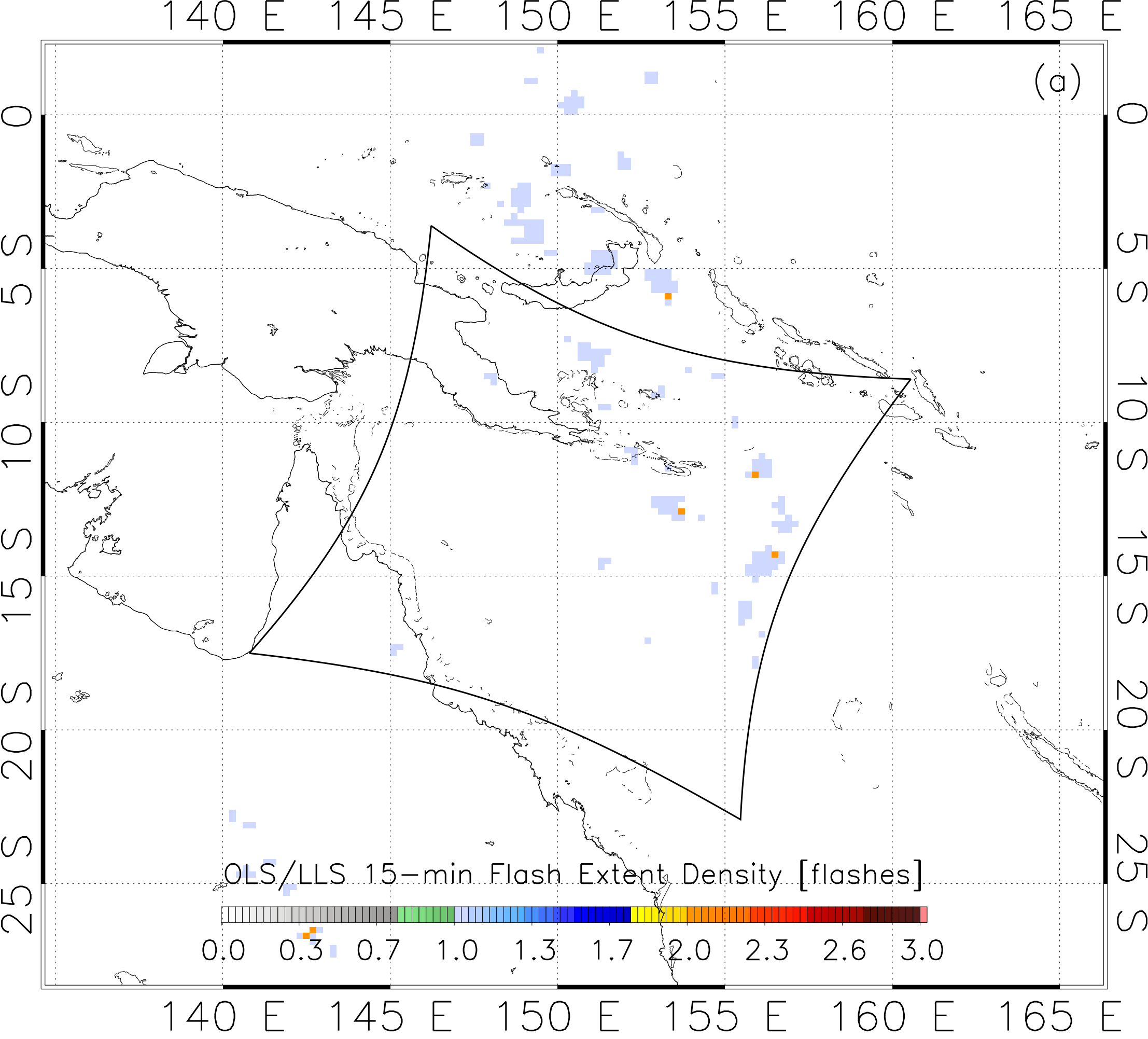


Figure 3.

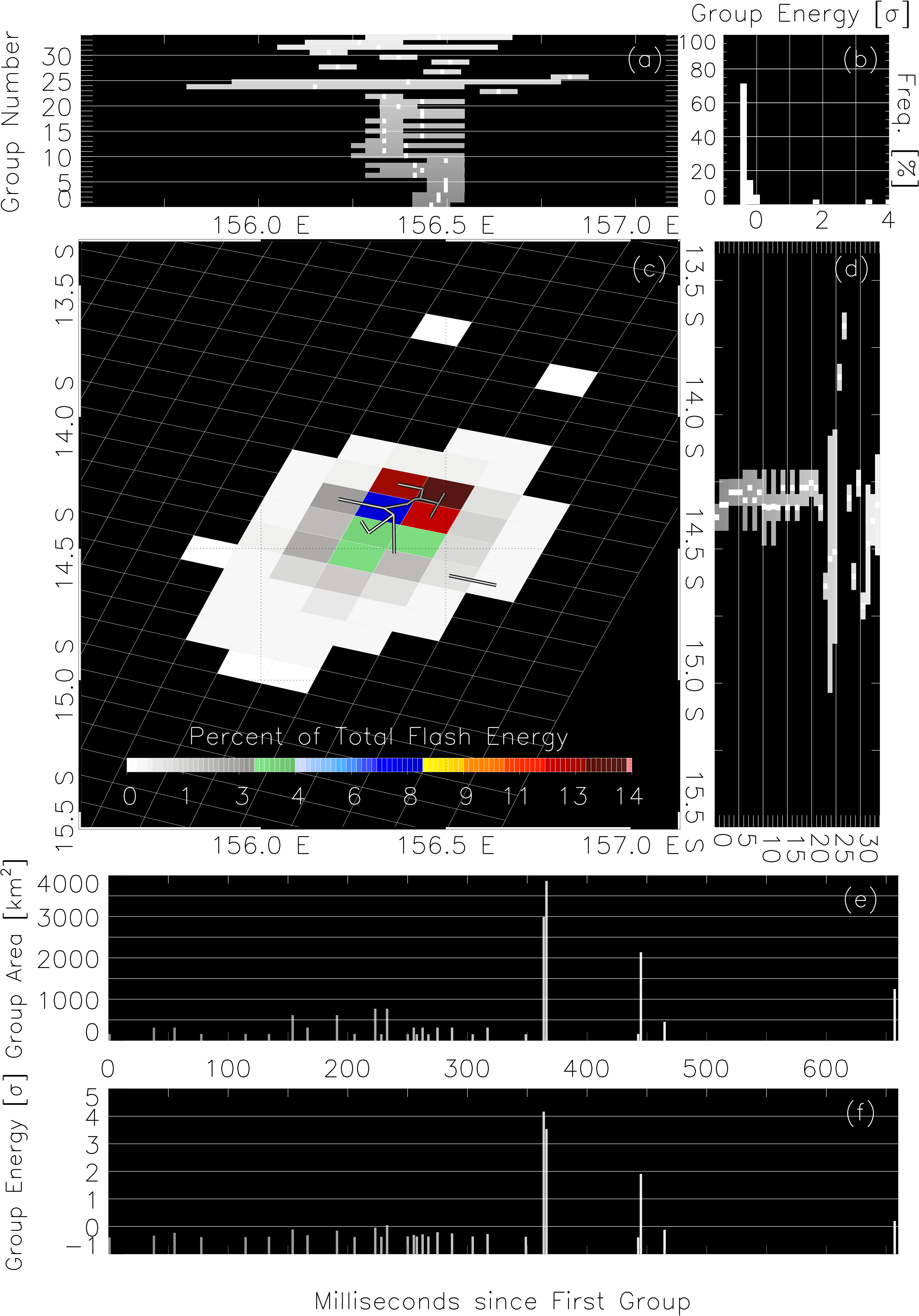


Figure 4.

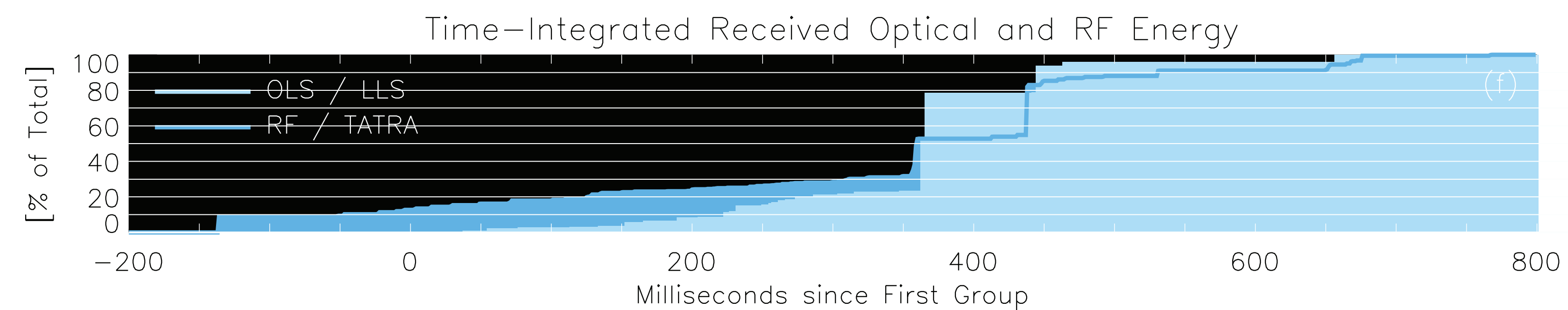
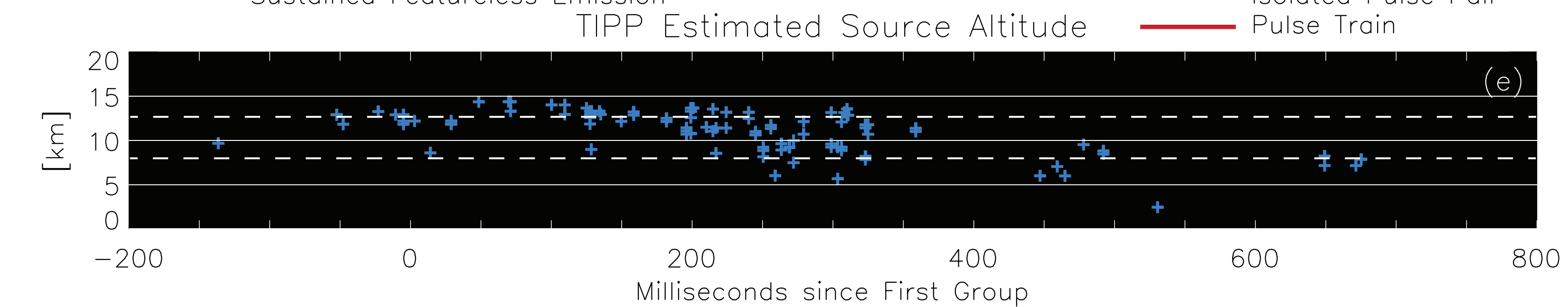
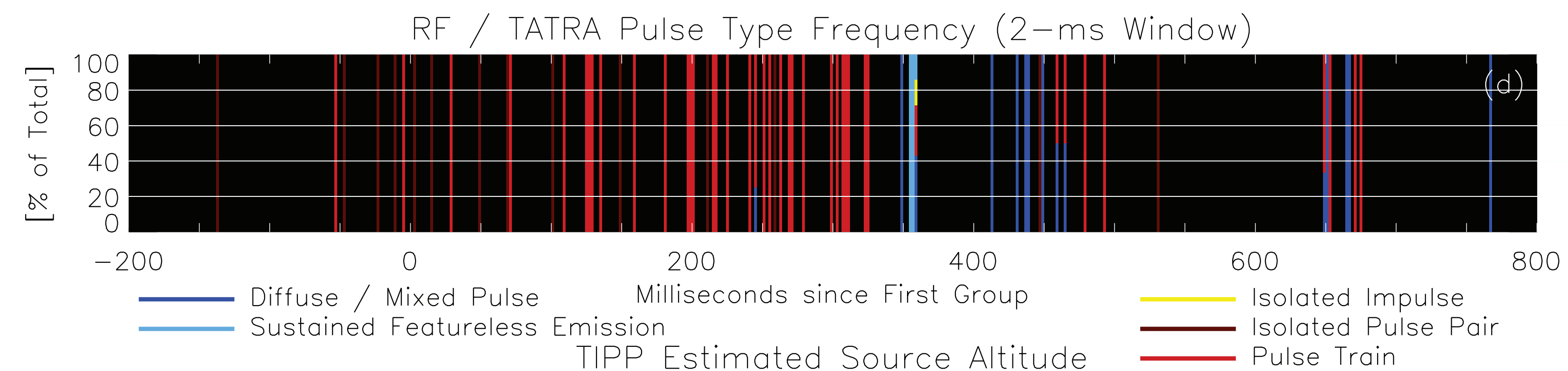
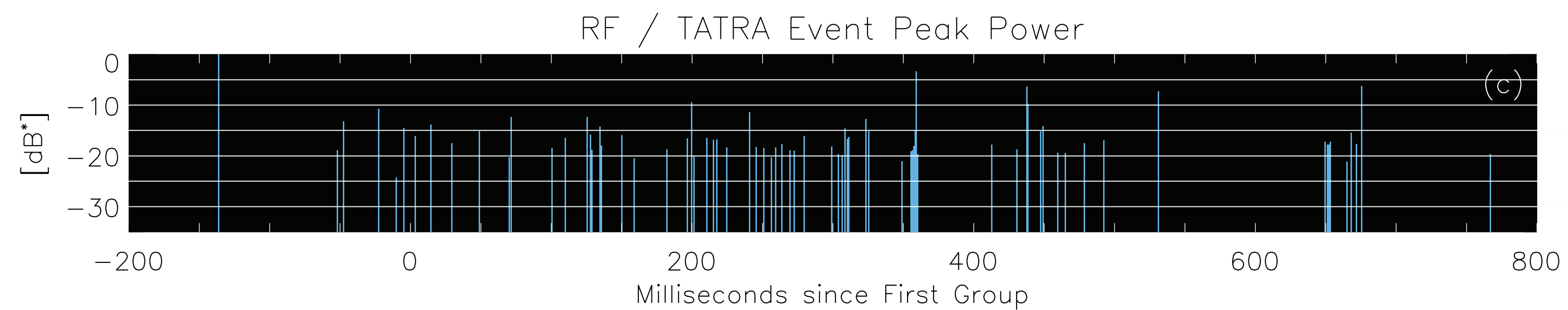
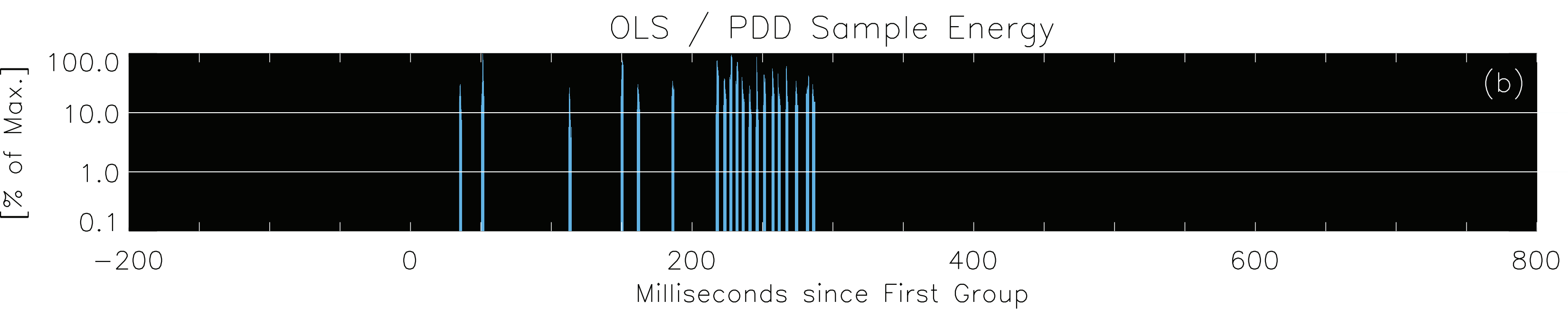
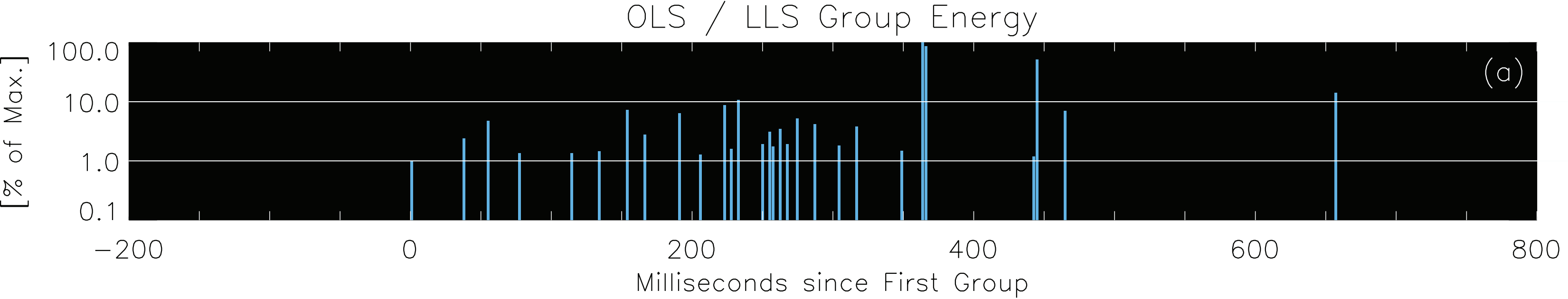


Figure 5.

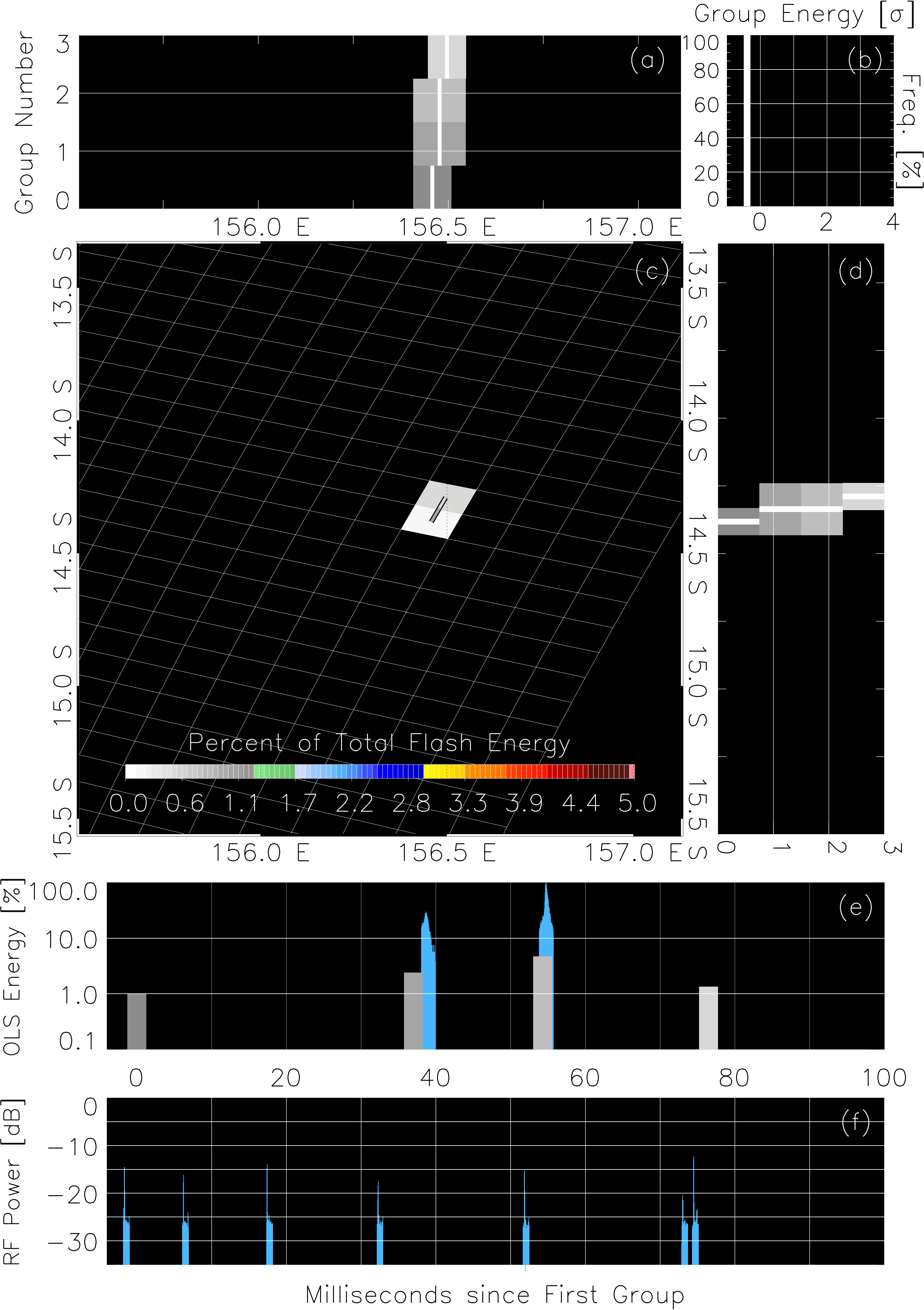


Figure 6.

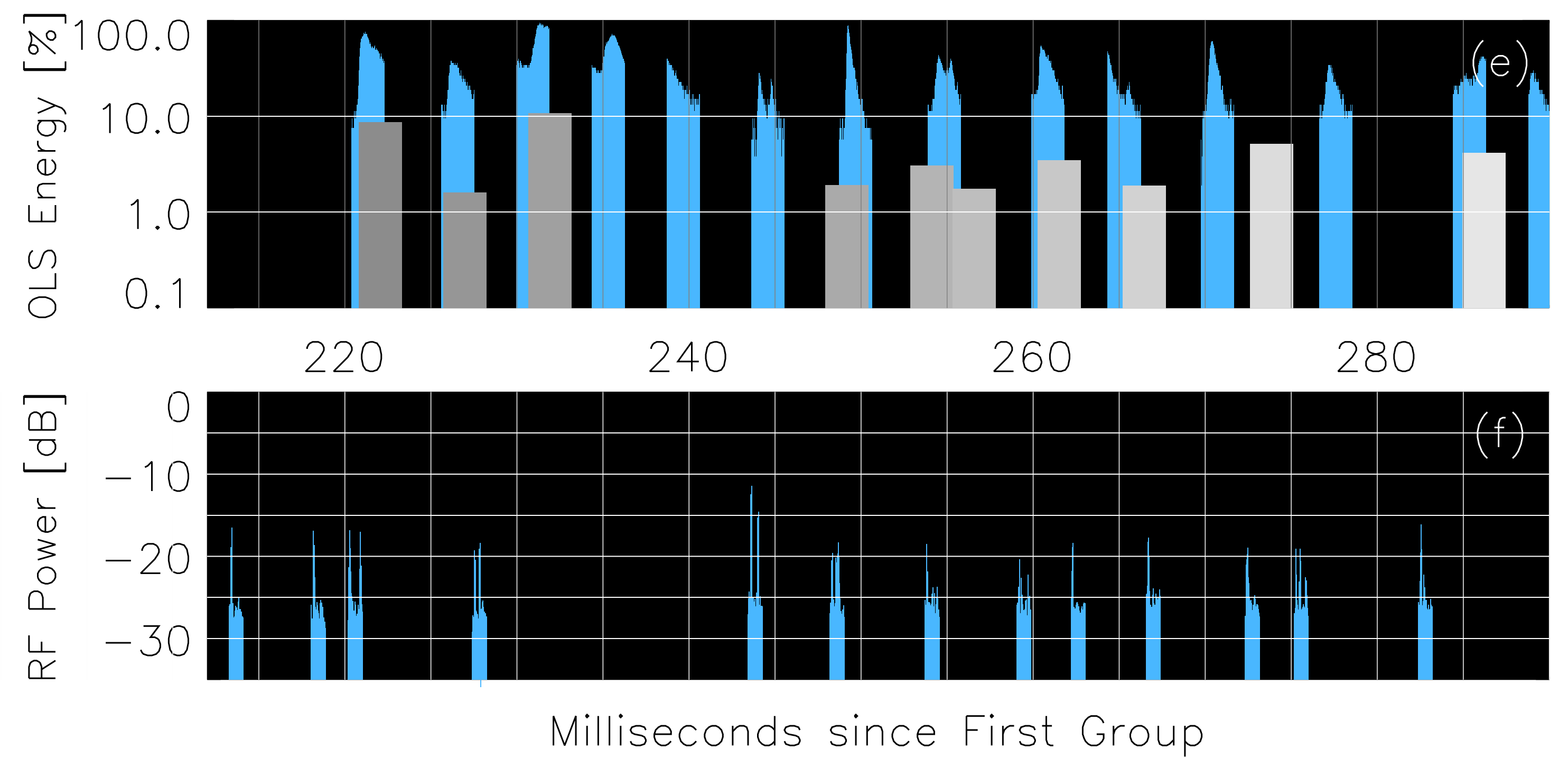
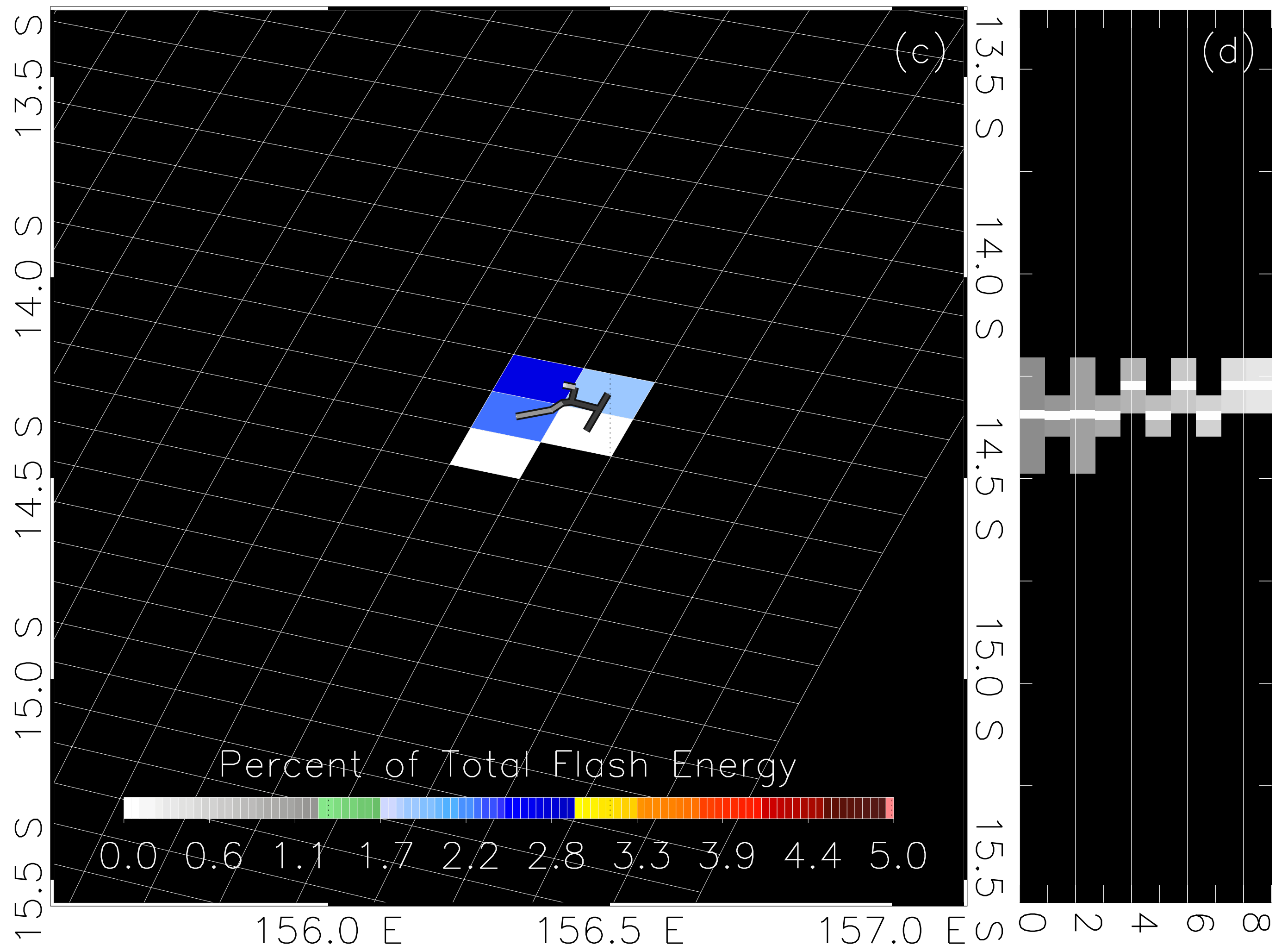
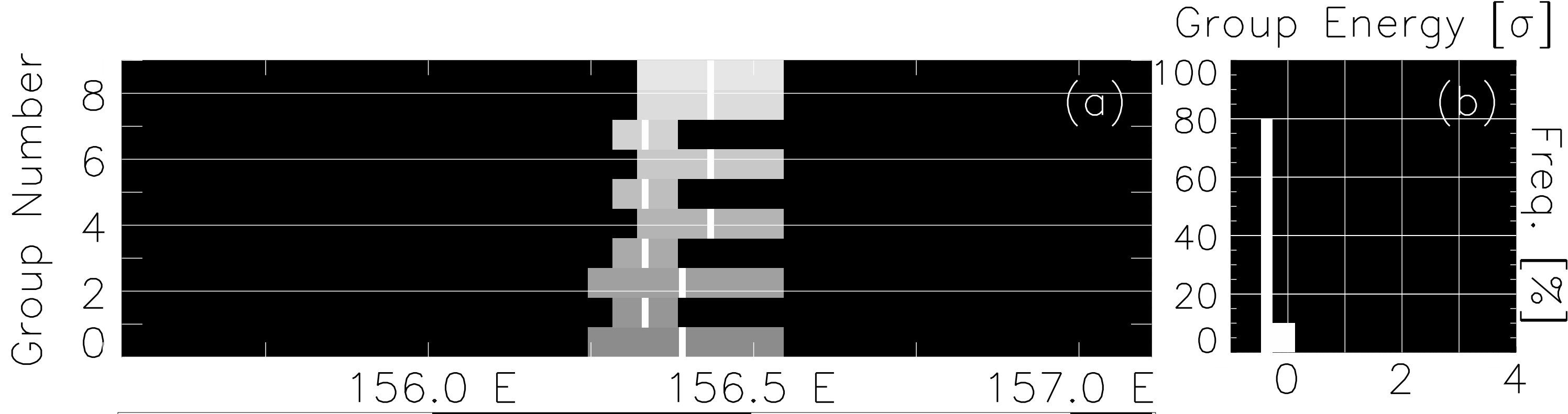


Figure 7.

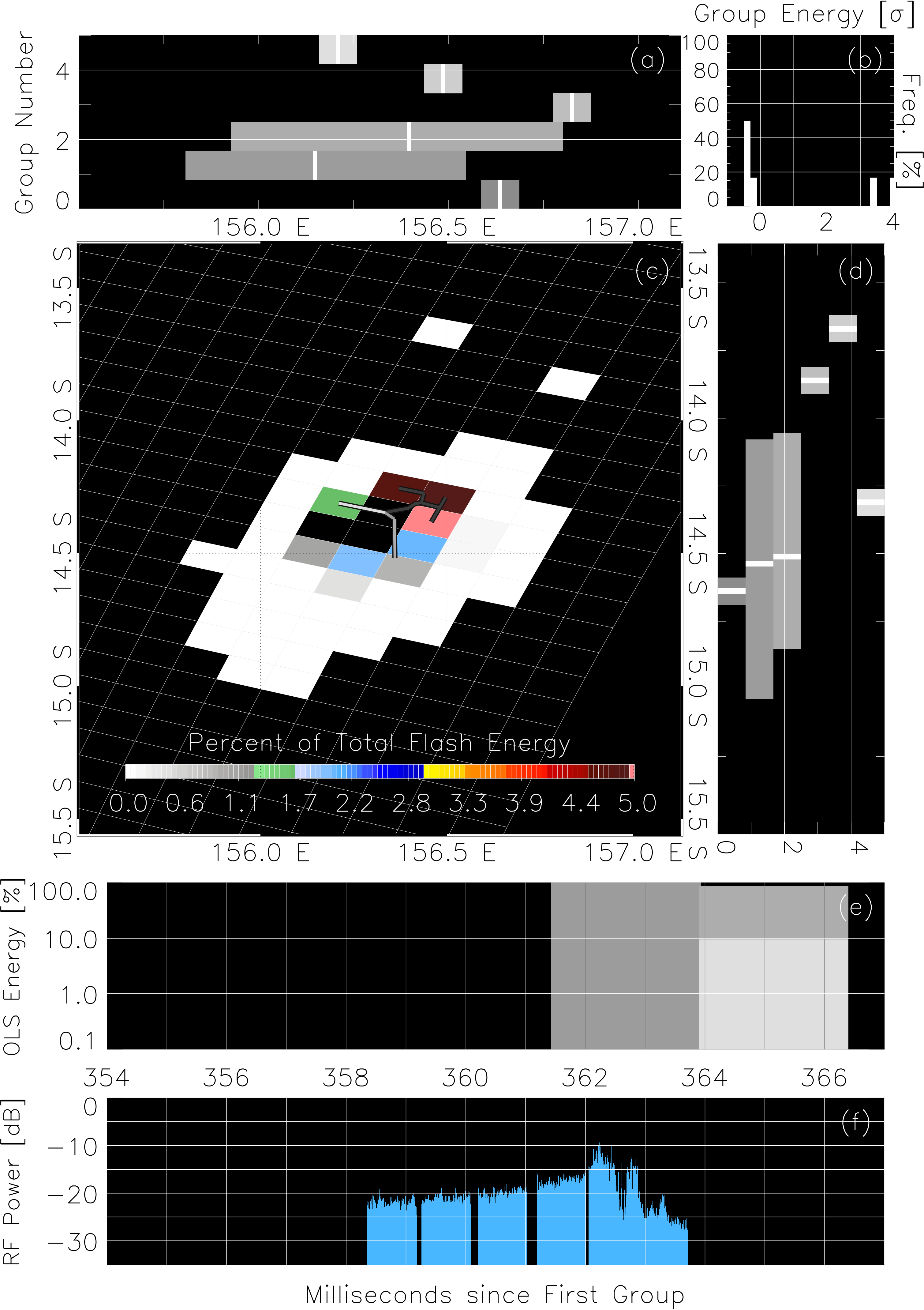


Figure 8.

